Mechanically modulated emission spectra and blockade of polaritons in a hybrid semiconductor-optomechanical system

Sai-Nan Huai,[1] Yu-Long Liu,[1] Yunbo Zhang,[2] and Yu-xi Liu[1,3,*]
[1]*Institute of Microelectronics, Tsinghua University, Beijing 100084, China*
[2]*Institute of Theoretical Physics, Shanxi University, Taiyuan 030006, China*
[3]*Tsinghua National Laboratory for Information Science and Technology (TNList), Beijing 100084, China*

(Received 15 March 2018; published 26 September 2018)

We study a hybrid semiconductor-optomechanical system, which consists of a cavity with an oscillating mirror made by semiconducting materials or with a semiconducting membrane inside. The cavity photons and the excitons in the semiconducting oscillating mirror or membrane form into polaritons. Thus, the optomechanical interaction between the cavity photons and the mirror or membrane is changed into the polariton-mechanical interaction. We theoretically study the eigenvalues and eigenstates of this tripartite system with the generalized rotating-wave approximation. We show the mechanical-resonator-modulated emission spectra of polariton modes. We also analyze the mechanical effect on the statistical properties of the polariton when the cavity is driven by a weak classical field. This work provides a detailed description of the rich nonlinearity, which is resulted from the competition between parametric coupling and three-wave mixing interaction concerning the polariton modes and the phonon mode. It also offers a way to operate the photons, phonons, and excitons in the integrated semiconducting-optomechanical platform.

DOI: 10.1103/PhysRevA.98.033825

I. INTRODUCTION

Cavity optomechanical systems, which consist of single-mode cavity fields and mechanical resonators, have attracted growing interest for their potential applications in ultrasensitive force sensors, frequency conversion, high-precision measurements, and quantum information processing [1–6]. They can also be used to realize more complex tasks by coupling to other systems. For example, there are studies that optomechanical systems are coupled to either two-level or other systems via either cavity fields [7–15] or mechanical resonators [16–19], and even both of them [20]. Various materials are used or proposed to construct optomechanical systems in order to increase or control optomechnaical coupling. However, material properties of cavities and mechanical resonators in these studies are less studied.

It is known that many optomechanical systems are made of semiconducting materials, for example, cavity optomechanics was demonstrated in gallium arsenide [21–26] and gallium phosphide microdisks [27]. Recently, there are reports on the coupling between excitons (electron-hole pairs) and mechanical resonator, in GaAs/AlGaAs quantum dot systems [28,29]. Also, an optomechanical experiment showed that the mechanical modes of a GaAs nanomembrane can be cooled down via photothermal effect mediated by excitons inside the membrane [26]. Moreover, cavityless optomechanics is demonstrated by virtue of optopiezoelectric back-action through excitons in an n-GaAs/i-GaAs bilayer cantilevers [30,31]. Such carrier mediated optomechanical coupling does not require any optical cavities but is based on the piezoelectric effect. In addition, an approach to optically access the dark excitons using a time-varying strain to a n-$Al_{0.3}Ga_{0.7}As$/i-GaAs micromechanical resonator is studied experimentally [32].

Besides, semiconducting microcavity quantum electrodynamics (QED) is extensively studied since the observation of the strong coupling between a single-mode cavity field and excitons in semiconducting quantum well [33–36]. It is well known that the strong coupling between the excitons and photons mix them into the so-called polaritons [37]. In low-dimensional semiconductor [38–41] or semiconducting cavity QED [42,43] systems, the polaritons can be observed through photoluminescence, photon reflection, or transmission. Recently, cavity polariton optomechanics has been demonstrated and the polariton-mediated strong light-sound interaction was shown [44,45]. Moreover, unconventional bistability in optomechanical system with cavity polariton [46] and exciton-phonon entanglement [47] was also studied.

All of these studies [44–47] open up a way to operate photons, excitons, and phonons in an integrated semiconducting platform utilizing semiconducting microcavity QED and optomechanics. For example, the spectrum of mechanical oscillation is proposed to detect the fine energy structure of the excitons in semiconducting materials, in the way of measuring the wavelength dependence of thermal-mechanical vibration of the mechanical resonator [23,30,31]. As shown in Ref. [23], the ability to detect small but sharp photoabsorption peaks allows the mechanically resolved photoabsorption measurement to offer a complement to the existing photoabsorption measurements that directly measure absorption intensities. Motivated by these works [24,26,30,31,44–46], here we study a hybrid system combining the semiconducting microcavity quantum electrodynamics with optomechanics. The system consists of a cavity with an oscillating mirror made by

*yuxiliu@mail.tsinghua.edu.cn

semiconducting materials or with a semiconducting membrane inside the cavity. We will show how the mechanical motion affects the emission spectra and blockade of polaritons.

The paper is organized as follows. In Sec. II, we will describe a theoretical model for the interaction between the exciton, a single-mode cavity field, and the mechanical resonator. In Sec. II A, we introduce the polariton modes formed by the cavity photons and excitons. In Sec. II B, we first present general method to get the eigenvalues of the hybrid system, and then as an example, we analyze eigenvalues and eigenstates of one polariton subspace for fully coupled hybrid system by diagonalizing the system Hamiltonian with the generalized rotating-wave approximation (GRWA) proposed in Ref. [48]. In Sec. III, we study the emission spectra of the polaritons and show how the mechanical resonator affects the properties of the spectra. In Sec. IV, the statistic properties of the polaritons are investigated via the equal-time second-order correlation function, and furthermore the polariton blockade and tunneling are discussed. Finally, we summarize our research results in Sec. V. For the compactness and completeness of the paper, the details about Schwinger's representations of the Hamiltonian, the eigenvalues in the one- and two-polariton subspaces are shown in Appendices A, B, and C, respectively.

II. MODEL

As schematically shown in the left parts of Fig. 1, we study a hybrid cavity polariton optomechanical system that consists of a cavity either with an oscillating mirror made of semiconducting materials in Fig. 1(a) or a semiconducting membrane placed in the middle of the cavity in Fig. 1(b). In the right parts of Figs. 1(a) and 1(b), we also show the coupling relationship corresponding to the left ones. The difference between these two situations, shown in Figs. 1(a) and 1(b), is whether there is direct coupling between the excitons in the semiconductor and the mechanical resonator, while we assume that the couplings of the photons to excitons and phonons exist in both configurations. The Hamiltonian of the whole system can be written as ($\hbar = 1$)

$$H = \omega_c a^\dagger a + \omega_m b^\dagger b + \omega_{\rm ex} c^\dagger c + g_0 a^\dagger a(b^\dagger + b) + \lambda c^\dagger c(b^\dagger + b) + \eta(a^\dagger c + c^\dagger a), \quad (1)$$

where a ($a^\dagger$), b ($b^\dagger$), and c ($c^\dagger$) are the annihilation (creation) operators of the cavity field, mechanical resonator, and exciton, with corresponding resonant frequencies ω_c, ω_m, and ω_{ex}, respectively. The first line in Eq. (1) shows the free Hamiltonian of the system, while the rest terms describe the interaction in the fully coupled tripartite hybrid system. The parameter $g_0 = \omega_c x_{\rm zpf}/L$ represents the single photon-phonon coupling constant caused by the radiation pressure between the cavity field and the oscillating mirror (or vibrating membrane), where $x_{\rm zpf}$ is the mechanical zero-point fluctuation and L is the length of the cavity. The parameter λ denotes the coupling between the exciton and mechanical resonator, while η describes the interaction between the cavity photon and the exciton with rotating-wave approximation. For the case shown in Fig. 1(a), we assume that the oscillating mirror made of semiconducting materials moves in translation, and there is no direct coupling between the exciton and the phonon, i.e., $\lambda = 0$. However, for the drumlike vibrations shown in Fig. 1(b), the coupling constant between the exciton and the mechanical modes is nonzero, i.e., $\lambda \neq 0$, as a result of the piezoelectric effect. In our paper, we will study the model shown in Fig. 1(b) for generality and regard $g_0 = \lambda$ as the balanced coupling case. Our research results can be applied to the case shown in Fig. 1(a) by setting $\lambda = 0$.

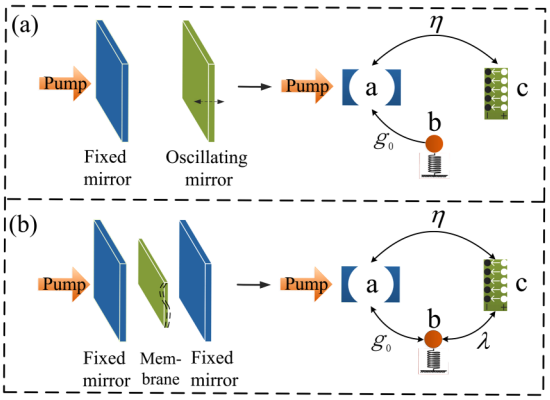

FIG. 1. Schematic diagram of a hybrid semiconducting cavity optomechanical system with (a) an oscillating mirror made by the semiconducting materials or (b) a thin semiconducting membrane inside the cavity. In each panel, the right part further shows the coupling relation between the three parts of the hybrid system, which consists of the photons confined in the cavity, excitons in the semiconducting materials, and phonons in the oscillating resonator. In the right parts of both (a) and (b), the cavity is denoted by blue square brackets with the letter "a" inside. The excitons are presented by pairs of black (denoting the electrons) and white dots (denoting holes) with the letter "c," which are attracted to each other by the Coulomb interaction. Mechanical oscillator is denoted by a ball bounded to a spring with the letter "b." The parameters η, g_0, and λ represent the cavity photon-exciton, photon-phonon, and exciton-phonon coupling constants, respectively. We assume (i) the mirror in (a) moves in translation; (ii) the membrane in (b) has drumlike vibration; (iii) there is no direct coupling between the exciton and mechanical resonator in (a).

A. Polariton modes

When the photons are coupled to the excitons, the cavity and exciton modes are hybridized into polariton modes, which can be expressed as [37]

$$\begin{pmatrix} A \\ B \end{pmatrix} = \begin{pmatrix} \cos\theta & \sin\theta \\ -\sin\theta & \cos\theta \end{pmatrix} \begin{pmatrix} a \\ c \end{pmatrix}.$$

Here, $\tan 2\theta = 2\eta/\Delta_{ce}$ and $\theta \in [0, \pi/2]$, with $\Delta_{ce} = \omega_{ex} - \omega_c$, which is the detuning between the exciton and the photon. This transformation shows that the photonic and excitonic components vary a lot in polariton modes A and B for different detuning Δ_{ce} and coupling constant η between the photon and the exciton. When the detuning Δ_{ce} is very large, the polariton mode A approaches either bare cavity (positive infinite detuning) or exciton mode (negative infinite detuning), and vice versa for mode B. However, for the resonant case with $\Delta_{ce} = \omega_{ex} - \omega_c = 0$, $\theta = \pi/4$, we can get the maximally

hybridized polariton modes $A/B = (c \pm a)/\sqrt{2}$, where A (B) mode corresponds to the sign + (−). Using the polariton modes, we can rewrite the total Hamiltonian in Eq. (1) as

$$\begin{aligned} H_0 = {} & \omega_A A^\dagger A + \omega_B B^\dagger B + \omega_m b^\dagger b \\ & + (Q_A A^\dagger A + Q_B B^\dagger B)(b^\dagger + b) \\ & + Q(A^\dagger B + B^\dagger A)(b^\dagger + b). \end{aligned} \tag{2}$$

Here, ω_A and ω_B are the eigenvalues of the polariton modes A and B with

$$\omega_{A/B} = \frac{1}{2}(\omega_c + \omega_{ex}) \pm \frac{\eta}{\sin 2\theta}, \tag{3}$$

where the sign + (−) corresponds to ω_A (ω_B). Parameters Q_A, Q_B (Q) denote the parametric (three-wave mixing interaction) polariton-phonon coupling constants. These parameters can be expressed in terms of the parameters g_0, λ, and θ as

$$Q_A = g_0 \cos^2\theta + \lambda \sin^2\theta, \tag{4}$$

$$Q_B = g_0 \sin^2\theta + \lambda \cos^2\theta, \tag{5}$$

$$Q = (\lambda - g_0)\cos\theta \sin\theta. \tag{6}$$

We can find that the couplings between the polariton modes and mechanical mode are modified since the polariton modes are mixtures of both cavity field and exciton modes. We also note that, for large photon-exciton detuning with $\Delta_{ce} \gg \eta$ so that $\theta \approx 0$ (or the balanced coupling case with $g_0 = \lambda$), the three-wave mixing interaction $Q \approx 0$ ($Q = 0$) and there are only parametric couplings between the polariton modes and the phonon mode.

B. Eigenvalues and eigenstates

To have insight into the nature of the fully coupled tripartite system, we first study the eigenvalues and eigenstates of the Hamiltonian in Eq. (2). In terms of Schwinger's representation for two bosonic polariton modes A and B, the angular-momentum operators can be constructed as [49]

$$\begin{aligned} J_x &= \frac{1}{2}(A^\dagger B + B^\dagger A), \quad J_y = \frac{1}{2i}(A^\dagger B - B^\dagger A), \\ J_z &= \frac{1}{2}(A^\dagger A - B^\dagger B). \end{aligned} \tag{7}$$

The operators J_x, J_y, and J_z represent the X, Y, and Z components of the total angular-momentum operator J, which can be given as [49]

$$J^2 = J_x^2 + J_y^2 + J_z^2 = \frac{N}{2}\left(\frac{N}{2} + 1\right). \tag{8}$$

Here, $N = A^\dagger A + B^\dagger B$ denotes the total polariton number operator of modes A and B. Then, the Hamiltonian in Eq. (2) can be rewritten as

$$\begin{aligned} H_1 = {} & \tfrac{1}{2}(\omega_A + \omega_B)N + (\omega_A - \omega_B)J_z + \omega_m b^\dagger b \\ & + \left(\Omega N + G e^{i\phi J_y} J_z e^{-i\phi J_y}\right)(b^\dagger + b), \end{aligned} \tag{9}$$

Other parameters are given by

$$\Omega = \tfrac{1}{2}(Q_A + Q_B), \quad \phi = 2\theta, \quad G = g_0 - \lambda. \tag{10}$$

For the large photon-exciton detuning ($\Delta_{ce} \gg \eta$, then $\phi \approx 0$) or the balanced coupling ($g_0 = \lambda$, then $G = 0$) case, i.e., when there are only parametric couplings between the polariton modes and the phonon mode, we can apply a unitary transformation

$$U_2 = \exp[(\Omega N + G J_z)(b^\dagger - b)/\omega_m] \tag{11}$$

to the Hamiltonian in Eq. (9). This transformation displaces the creation and annihilation operators of the mechanical resonator by $(\Omega N + G J_z)/\omega_m$. Then, Eq. (9) can be transformed into

$$\begin{aligned} \tilde{H}_2 = {} & \frac{1}{2}(\omega_A + \omega_B)N + (\omega_A - \omega_B)J_z + \omega_m b^\dagger b \\ & - \frac{1}{\omega_m}(\Omega N + G J_z)^2. \end{aligned} \tag{12}$$

Thus, the eigenvalues of the system can be approximately obtained as

$$\begin{aligned} E_{j,m,n_b} = {} & j(\omega_A + \omega_B) + m(\omega_A - \omega_B) + n_b\omega_m \\ & - \frac{1}{\omega_m}(2\Omega j + Gm)^2 \end{aligned} \tag{13}$$

when $\phi \approx 0$ or $G = 0$. The eigenstates corresponding to Eq. (12) can also be given by

$$\psi_{j,m,n_b} = |j, m\rangle |n_b\rangle_{j,m}. \tag{14}$$

Here, (j, m) are the quantum numbers labeling the simultaneous eigenstates $|j, m\rangle$ of the angular momentum operators J^2 and J_z, whose detailed description can be referred to Appendix A. The angular quantum numbers can be obtained as $j = \mathcal{N}/2$, $m = -\mathcal{N}/2, \ldots, \mathcal{N}/2$, according to Eqs. (7) and (8), with the parameter $\mathcal{N}$ denoting the total polariton number corresponding to the total polarition number operator N. The parameter n_b denotes the phonon excitation number corresponding to the phonon number operator $N_b = b^\dagger b$, i.e., $N_b|n_b\rangle = n_b|n_b\rangle$, while the state

$$|n_b\rangle_{j,m} = e^{-\beta_{j,m}(b^\dagger - b)}|n_b\rangle \tag{15}$$

represents a (j, m) polariton displaced Fock state [50] with the displacement $\beta_{j,m} = (\mathcal{N}\Omega + mG)/\omega_m$. The last term in Eq. (13) describes the frequency shifts and the nonlinearity of the polariton modes, caused by the parametric coupling to the phonon mode b.

However, for the most common case in which the three-wave mixing interaction is involved, i.e., when $\phi \neq 0$ and $G \neq 0$, Eq. (9) can be transformed into [51,52]

$$\begin{aligned} H_2 = {} & \tfrac{1}{2}(\omega_A + \omega_B)N + (\omega_A - \omega_B)(\cos\phi J_z + \sin\phi J_x) \\ & + \omega_m N_b + (\Omega N + G J_z)(b^\dagger + b) \end{aligned} \tag{16}$$

by performing a rotation $U_1 = \exp(-i\phi J_y)$. In order to tackle the static shift of the mechanical resonator equilibrium position caused by polaritons, we apply the unitary transform U_2, which is shown in Eq. (11), to Eq. (16). Then, we obtain an

effective Hamiltonian

$$H_3 = \frac{1}{2}(\omega_A + \omega_B)N + (\omega_A - \omega_B)\cos\phi J_z + \omega_m N_b + (\omega_A - \omega_B)\sin\phi J_x \cosh\left[\frac{G}{\omega_m}(b^\dagger - b)\right] + i(\omega_A - \omega_B)\sin\phi J_y \sinh\left[\frac{G}{\omega_m}(b^\dagger - b)\right] - \frac{1}{\omega_m}(\Omega N + G J_z)^2. \quad (17)$$

It is clear that the effective Hamiltonian in Eq. (12) for the $\phi = 0$ case can be arrived by setting $\phi = 0$ in Eq. (17) directly, and the effective Hamiltonian with $G = 0$ in Eq. (12) can also be obtained by performing an inverse transformation $U_1^\dagger = \exp(i\phi J_y)$ to Eq. (17) with $G = 0$.

The three-wave mixing interaction included in the second and third lines of Eq. (17) plays an important role for the common case, and its competition with the parametric coupling will surely induce more abundant nonlinear phenomena. We can expand the hyperbolic functions cosh and sinh, respectively, as

$$\cosh\left[\frac{G}{\omega_m}(b^\dagger - b)\right] = G_0(N_b) + G_1(N_b)b^{\dagger 2} + b^2 G_1(N_b) + \cdots, \quad (18)$$

$$\sinh\left[\frac{G}{\omega_m}(b^\dagger - b)\right] = F_1(N_b)b^\dagger - bF_1(N_b) + F_2(N_b)b^{\dagger 3} - b^3 F_2(N_b) + \cdots. \quad (19)$$

Here, $G_i(N_b)$ $(i = 0, 1, \dots)$ and $F_j(N_b)$ $(j = 1, 2, \dots)$ are coefficients that depend on the phonon number operator $N_b = b^\dagger b$ and the dimensionless parameter G/ω_m. Different orders of approximations can be performed by only keeping resonant terms while neglecting others in the expansions. The zeroth-order approximation of the Hamiltonian, whose validity has been shown to be restricted to the large detuning regime, i.e., $(\omega_A - \omega_B)\cos\phi \ll \omega_m$ [53–56], can be obtained by only keeping $G_0(N_b)$ but neglecting the phonon exchange terms in the expansion of Eq. (17). However, for the resonant case we considered in this work, i.e., $(\omega_A - \omega_B)\cos\phi = \omega_m$, single-phonon exchange terms $F_1(N_b)b^\dagger$, $bF_1(N_b)$ should be taken into account in the first-order approximation [57,58].

We note that the total polariton number operator N commutes with the total Hamiltonian of the system, i.e., $[H_3, N] = 0$, thus the Hamiltonian of the closed system can be block-diagonalized in the basis of the eigenstates of the polariton number operator. When there is no polariton excitation, i.e., $\mathcal{N} = 0$, the eigenvalue behaves just like the usual harmonic structure. As shown in Fig. 2(c), it reveals that the eigenvalues are independent of the coupling constant g_0 between the cavity field and mechanical resonator.

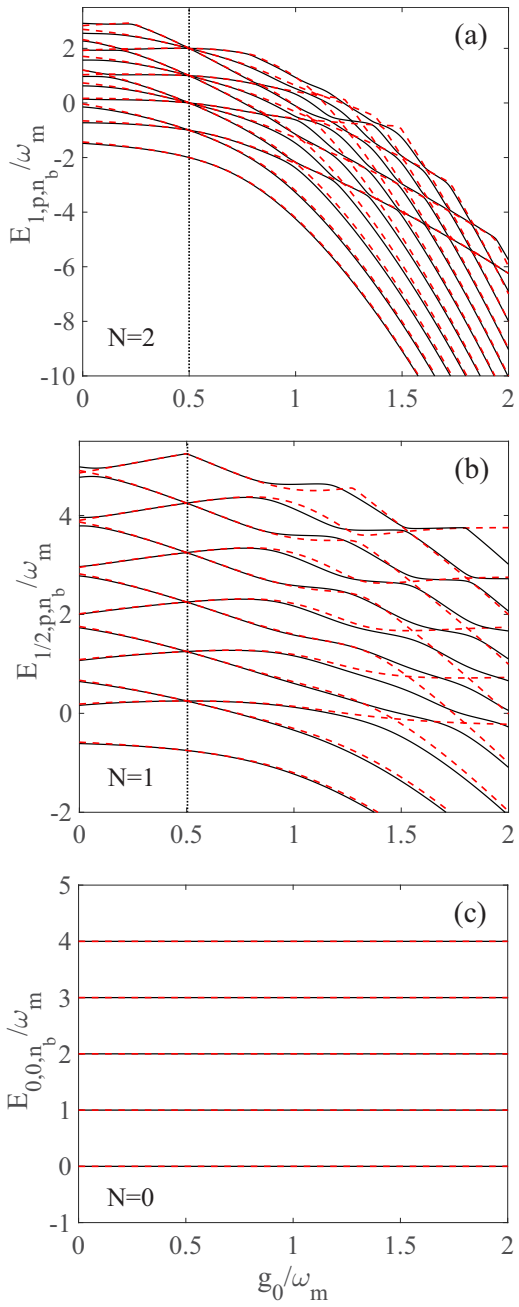

FIG. 2. Energy levels of the system for polariton excitation numbers (a) $\mathcal{N} = 2$, (b) $\mathcal{N} = 1$, (c) $\mathcal{N} = 0$ versus the coupling strength g_0/ω_m when the cavity field resonantly interacts with excitons, i.e., $\Delta_{ce} = 0$. The black-solid curves represent the numerical result while the red-dashed curves are following the GRWA results. Specifically, the red-dashed curves in (a) correspond to the results shown in Eqs. (C18), (C20) and (C21), while they are referred to Eqs. (24) and (27) in (b). Other parameters are $\eta = 0.5\,\omega_m$, $\lambda = 0.5\,\omega_m$.

For the $\mathcal{N} = 1$ subspace, J_x, J_y, and J_z are defined in two-dimensional space and equivalent to Pauli operators, i.e., $J_x = \sigma_x/2$, $J_y = \sigma_y/2$, and $J_z = \sigma_z/2$. As shown in the Appendix B, by applying a unitary transformation

$$U_3 = \begin{bmatrix} \frac{1}{\lambda_-} & \frac{\mu_-}{\lambda_-} \\ \frac{1}{\lambda_+} & \frac{\mu_+}{\lambda_+} \end{bmatrix} \quad (20)$$

to its angular-momentum part, the total Hamiltonian in Eq. (17) with single-phonon exchange terms can be reduced to

$$\begin{aligned} H_3^{\mathrm{GRWA}} &= \omega_m N_b + \xi_{-,N_b}\left|\frac{1}{2},-\frac{1}{2}\right\rangle\left\langle\frac{1}{2},-\frac{1}{2}\right| \\ &\quad + \xi_{+,N_b}\left|\frac{1}{2},\frac{1}{2}\right\rangle\left\langle\frac{1}{2},\frac{1}{2}\right| \\ &\quad + \mathcal{P}_{N_b} b^\dagger\left|\frac{1}{2},-\frac{1}{2}\right\rangle\left\langle\frac{1}{2},\frac{1}{2}\right| \\ &\quad + \mathcal{P}_{N_b} b\left|\frac{1}{2},\frac{1}{2}\right\rangle\left\langle\frac{1}{2},-\frac{1}{2}\right|, \end{aligned} \tag{21}$$

with the generalized rotating-wave approximation (GRWA) [48]. Here, the phonon-number-dependent parameters are given by

$$\xi_{\pm,N_b} = \varepsilon_\pm + \frac{\mu_\pm}{\lambda_\pm^2}(\omega_A-\omega_B)\sin\phi[G_0(N_b)-\beta] \tag{22}$$

and

$$\mathcal{P}_{N_b} = \tfrac{1}{2}M_{12}(\omega_A-\omega_B)\sin\phi F_1(N_b). \tag{23}$$

Note here we have neglected the energy baseline $(\omega_A+\omega_B)/2$ for the sake of clarity and simplicity. The parameters $\lambda_\pm$, $\mu_\pm$, $\varepsilon_\pm$, M_{12} are defined in Appendix B. The superscript GRWA refers to the fact that the rotating-wave approximation is made after performing the first-order correction. The rotating-wave term for the expansion of $i\sigma_y \sinh[G(b^\dagger-b)/\omega_m]$ in Eq. (17) is exhibited in the energy-conserving terms $b|\frac{1}{2},\frac{1}{2}\rangle\langle\frac{1}{2},-\frac{1}{2}| + \mathrm{H.c.}$ with phonon-number-dependent coupling strength $\mathcal{P}_{N_b}$. In the n_bth subspace with the basis of $|\frac{1}{2},-\frac{1}{2},n_b\rangle$ and $|\frac{1}{2},\frac{1}{2},n_b-1\rangle$ $(n_b=1,2,\dots)$, the eigenvalues of the system can be given as

$$\begin{aligned} E^{\mathrm{GRWA}}_{\frac{1}{2},p,n_b} &= \left(n_b-\frac{1}{2}\right)\omega_m + \frac{1}{2}(\xi_{-,n_b}+\xi_{+,n_b-1}) \\ &\quad \pm\frac{1}{2}\sqrt{(\omega_m+\xi_{-,n_b}-\xi_{+,n_b-1})^2+4\mathcal{P}^2}, \end{aligned} \tag{24}$$

with the parameters $\xi_{\pm,n_b} = \langle n_b|\xi_{\pm,N_b}|n_b\rangle$, $\mathcal{P} = \langle n_b|\mathcal{P}_{N_b}|n_b-1\rangle$. The subscript $p=+$ or $p=-$ denotes the upper and lower eigenvalues, respectively. Meanwhile, the corresponding eigenstates in the n_bth subspace of the Hamiltonian H_3^{GRWA} are given by

$$\left|\varphi^{\mathrm{GRWA}}_{\frac{1}{2},p,n_b}\right\rangle = \frac{1}{t_{\frac{1}{2},p,n_b}}\left(\left|\frac{1}{2},-\frac{1}{2},n_b\right\rangle + \nu_{\frac{1}{2},p,n_b}\left|\frac{1}{2},\frac{1}{2},n_b-1\right\rangle\right),$$

with

$$\nu_{\frac{1}{2},n_b,p} = \mathcal{P}^{-1}\left[E^{\mathrm{GRWA}}_{\frac{1}{2},p,n_b} - (n_b\omega_m+\xi_{-,n_b})\right], \tag{25}$$

$$t_{\frac{1}{2},p,n_b} = \sqrt{1+\nu^2_{\frac{1}{2},n_b,p}}. \tag{26}$$

Particularly, the energy for the ground-state $|\frac{1}{2},-\frac{1}{2},0\rangle$ is

$$E_G^{\mathrm{GRWA}} = \varepsilon_-. \tag{27}$$

Considering the fact that unitary transformations have nothing to do with the eigenvalues but change the eigenstates, thus the eigenstates of the Hamiltonian H_1 can be approximately obtained from that of Hamiltonian H_3^{GRWA}, by performing the conjugate unitary transformations correspondingly, as

$$\begin{aligned} \left|\psi^{\mathrm{GRWA}}_{\frac{1}{2},p,n_b}\right\rangle &= U_1^\dagger U_2^\dagger U_3^\dagger\left|\varphi^{\mathrm{GRWA}}_{\frac{1}{2},p,n_b}\right\rangle \\ &= U_1^\dagger\left|\frac{1}{2},-\frac{1}{2}\right\rangle\frac{1}{\lambda_-}\frac{1}{t_{\frac{1}{2},p,n_b}}|n_b\rangle_{\frac{1}{2},-\frac{1}{2}} \\ &\quad + U_1^\dagger\left|\frac{1}{2},-\frac{1}{2}\right\rangle\frac{1}{\lambda_+}\frac{\nu_{\frac{1}{2},n_b,p}}{t_{\frac{1}{2},p,n_b}}|n_b-1\rangle_{\frac{1}{2},-\frac{1}{2}} \\ &\quad + U_1^\dagger\left|\frac{1}{2},\frac{1}{2}\right\rangle\frac{\mu_-}{\lambda_-}\frac{1}{t_{\frac{1}{2},p,n_b}}|n_b\rangle_{\frac{1}{2},\frac{1}{2}} \\ &\quad + U_1^\dagger\left|\frac{1}{2},\frac{1}{2}\right\rangle\frac{\mu_+}{\lambda_+}\frac{\nu_{\frac{1}{2},n_b,p}}{t_{\frac{1}{2},p,n_b}}|n_b-1\rangle_{\frac{1}{2},\frac{1}{2}}, \end{aligned} \tag{28}$$

$$\left|\psi_G^{\mathrm{GRWA}}\right\rangle = U_1^\dagger U_2^\dagger\left|\frac{1}{2},-\frac{1}{2},0\right\rangle = U_1^\dagger\left|\frac{1}{2},-\frac{1}{2}\right\rangle|0\rangle_{\frac{1}{2},-\frac{1}{2}}. \tag{29}$$

Here, $|n_b\rangle_{\frac{1}{2},m} = \exp[-(\Omega+mG)(b^\dagger-b)/\omega_m]|n_b\rangle$ is the displaced Fock state, with the displacement $(\Omega+mG)/\omega_m$ determined by the quantum number m in the $\mathcal{N}=1$ subspace, and $m=\pm1/2$, $n_b=1,2,\dots$.

We have gotten all the eigenvalues for the $\mathcal{N}=1$ subspace with GRWA. This method can be extended to other subspaces with higher polariton excitation number $\mathcal{N}$. In the Appendix C, the eigenvalues $E^{\mathrm{GRWA}}_{1,q,n_b}$ in Eqs. (C18), (C20), and (C21) and eigenstates $|\psi^{\mathrm{GRWA}}_{1,q,n_b}\rangle$ in Eqs. (C22), (C23), and (C24) for the $\mathcal{N}=2$ subspace are also obtained.

In Fig. 2, the eigenvalues in the two-, one-, and zero-polariton subspace are plotted as a function of the photon-phonon coupling strength g_0 for given λ, respectively. In each panel, we have subtracted the base energy $j(\omega_A+\omega_B)$, with $j=\mathcal{N}/2$. The energy-level structures described by Eqs. (24) and (27) for the resonant case $\omega_c=\omega_{ex}$ are shown in red dashed curves, while the energy structures with the numerically exact diagonalization of the Hamiltonian in Eq. (16) for each polariton subspace are shown in black solid curves. The good agreement for $g_0<\omega_m$ between the theoretical method and numerical one shows the validity of GRWA in the regime we are working with. Discrepancies appear with the increase of the difference $|G|=|g_0-\lambda|$ between the photon-phonon and exciton-phonon coupling strengths. That is, for given λ (e.g., $\lambda=0.5\,\omega_m$ in Fig. 2), discrepancies appear when g_0 approaches 0 or surpasses $1\,\omega_m$, i.e., $|G|$ becomes larger than $0.5\,\omega_m$. They are mainly caused by the overlooked Stark effect and higher-order phonon transitions. It is obvious that the energy levels display much more abundant nonlinearity compared to the large photon-exciton detuning case as shown in Eq. (13), which is caused by the competition between the parametric coupling and three-wave mixing interaction concerning the polariton modes and phonon mode. What is more, as shown in the vertical black dotted line in Figs. 2(a) and 2(b), the specific photon-phonon coupling strength g_0, where the energy gap $E^{\mathrm{GRWA}}_{\frac{1}{2},+,n_b} - E^{\mathrm{GRWA}}_{\frac{1}{2},-,n_b}$ [Eq. (24)] in the same

n_bth manifold has the minimum value, is extremely close to the exciton-phonon coupling strength λ. If we further assume $|2\eta/\sin 2\theta| = \omega_m$, the gap is closed in the theoretical method, and the coupling strength g_0 equals λ. These phenomena can be used to detect the exciton-phonon coupling strength in the semiconducting cavity.

III. EMISSION SPECTRA OF THE POLARITONS

Let us now study the mechanical effect on the emission spectra of polaritons. There are many loss mechanisms involved in the dynamics of this hybrid system, including the mechanical damping rate γ_m, polariton emission rates κ_A and κ_B. However, in this section we only consider the simplest situation when the decay rates of the mechanical resonator and polariton modes are completely neglected. That is, we set $\gamma_m = \kappa_A = \kappa_B = 0$. Or, equivalently, we assume that the time length t of the excitation in the cavity satisfies the condition $1/\gamma \ll t \ll 1/\kappa_{A,B} \ll 1/\gamma_m$, where γ is the half-bandwidth of the spectrometer. In this case, it is also reasonable to neglect the three decay mechanisms. Thus, the only broadening mechanism comes from the detecting spectrometer, and its physical spectrum can be given by [59,60]

$$S(\omega) = 2\gamma \int_0^t dt_1 \int_0^t dt_2 \exp[-(\gamma - i\omega)(t - t_2)] \times \exp[-(\gamma + i\omega)(t - t_1)] G(t_1, t_2), \tag{30}$$

where $G(t_1, t_2)$ represents the dipole correlation function of the polaritons and is defined as

$$G(t_1, t_2) = \langle \psi(0)|B^\dagger(t_2)B(t_1)|\psi(0)\rangle \tag{31}$$

with $|\psi(0)\rangle$ the initial state of the system. Here, we take the lower-level polariton mode B as an example, and the analytic procedure can also be applied to the case of the mode A. Taking into account that the transition between different energy levels satisfies the condition

$$\langle j'm'|B|jm\rangle = \sqrt{j - m - 1}\,\delta_{j',j-\frac{1}{2}}\delta_{m',m+\frac{1}{2}}, \tag{32}$$

we can conclude the selection rule $j' = j - \frac{1}{2}$ and $m' = m + \frac{1}{2}$. And it is evident that j' is only determined by the initial state $|\psi(0)\rangle$. We first consider the case that the transition occurs between $\mathcal{N} = 1$ and 0 subspaces, and the mechanical resonator is in the displaced Fock state $|n_0\rangle_{\frac{1}{2},-\frac{1}{2}}$ initially. Thus, we make the assumption that the initial state of the system can be written as $|\psi(0)\rangle = |\frac{1}{2}, -\frac{1}{2}\rangle|n_0\rangle_{\frac{1}{2},-\frac{1}{2}}$. In fact, the method we used here is not restricted to our assumption of this particular initial state, but can be extended to more general case. The time-evolution operator $U(t)$ of the system concerning these subspaces can be gotten from the eigenvalues and eigenstates, i.e., Eqs. (24), (27), (28), and (29), which we have shown in the last section, that is,

$$U(t) = e^{-iH_1 t} = e^{-iE_G^{\mathrm{GRWA}}t}\left|\psi_G^{\mathrm{GRWA}}\right\rangle\left\langle\psi_G^{\mathrm{GRWA}}\right| + \sum_{p,n_b} e^{-iE_{\frac{1}{2},p,n_b}^{\mathrm{GRWA}}t}\left|\psi_{\frac{1}{2},p,n_b}^{\mathrm{GRWA}}\right\rangle\left\langle\psi_{\frac{1}{2},p,n_b}^{\mathrm{GRWA}}\right|. \tag{33}$$

Taking into account the fact that $B(t) = U^\dagger(t)BU(t)$, the correlation $G(t_1, t_2)$ can be obtained as

$$\begin{aligned} G(t_1, t_2) = &\sum_{n_1=0,n_2} e^{i(E_G^{\mathrm{GRWA}} - E_{00n_2}^{\mathrm{GRWA}})(t_2-t_1)} \\ &\times \left|\langle\psi(0)\left|\psi_G^{\mathrm{GRWA}}\right\rangle\right|^2 \left|\left\langle\psi_G^{\mathrm{GRWA}}\left|B^\dagger\right|\psi_{00n_2}\right\rangle\right|^2 \\ &+ \sum_{n_1>0,p,n_2} e^{i(E_{\frac{1}{2},p_1,n_1}^{\mathrm{GRWA}} - E_{00n_2}^{\mathrm{GRWA}})(t_2-t_1)} \\ &\times \left|\left\langle\psi(0)\left|\psi_{\frac{1}{2},p_1,n_1}^{\mathrm{GRWA}}\right\rangle\right|^2 \left|\left\langle\psi_{\frac{1}{2},p_1,n_1}^{\mathrm{GRWA}}\left|B^\dagger\right|\psi_{00n_2}\right\rangle\right|^2, \end{aligned}$$

with $|\psi_{00n_2}\rangle = |00\rangle|n_2\rangle$. Thus, the stationary spectrum can be decomposed into three parts as

$$S_B^{10}(\omega) = S_1(\omega) + S_2(\omega) + S_3(\omega), \tag{34}$$

where

$$\begin{aligned} S_1(\omega) &= \sum_{n_1=0,n_2} \Gamma_1(\omega)\left|\left\langle\psi(0)|\psi_G^{\mathrm{GRWA}}\right\rangle\right|^2 \times \left|\left\langle\psi_G^{\mathrm{GRWA}}\left|B^\dagger\right|\psi_{00n_2}\right\rangle\right|^2, \\ S_2(\omega) &= \sum_{n_1>0,n_2} \Gamma_2(\omega)\left|\left\langle\psi(0)|\psi_{\frac{1}{2},+,n_1}^{\mathrm{GRWA}}\right\rangle\right|^2 \times \left|\left\langle\psi_{\frac{1}{2},+,n_1}^{\mathrm{GRWA}}\left|B^\dagger\right|\psi_{00n_2}\right\rangle\right|^2, \\ S_3(\omega) &= \sum_{n_1>0,n_2} \Gamma_3(\omega)\left|\left\langle\psi(0)|\psi_{\frac{1}{2},-,n_1}^{\mathrm{GRWA}}\right\rangle\right|^2 \times \left|\left\langle\psi_{\frac{1}{2},-,n_1}^{\mathrm{GRWA}}\left|B^\dagger\right|\psi_{00n_2}\right\rangle\right|^2, \end{aligned}$$

with

$$\Gamma_i(\omega) = \frac{2\gamma}{\gamma^2 + [\omega - \omega_B - (\delta_i - n_2\omega_m)]^2}, \tag{35}$$

and $\delta_1 = \eta/\sin 2\theta + E_G^{\mathrm{GRWA}}$, $\delta_2 = \eta/\sin 2\theta + E_{\frac{1}{2},+,n_1}^{\mathrm{GRWA}}$, $\delta_3 = \eta/\sin 2\theta + E_{\frac{1}{2},-,n_1}^{\mathrm{GRWA}}$. Physically, this decomposition can be understood by the fact that the initial state $|\psi(0)\rangle = |\frac{1}{2}, -\frac{1}{2}\rangle|n_0\rangle_{\frac{1}{2},-\frac{1}{2}}$ is not the eigenstate of the Hamiltonian in Eq. (2), but it can always be interpreted as the superposition of the eigenstates $|\psi_G^{\mathrm{GRWA}}\rangle$ and $|\psi_{\frac{1}{2},p,n_1}^{\mathrm{GRWA}}\rangle$ ($p = \pm$). Moreover, the subscript in $S_B^{10}(\omega)$ denotes that this is the emission spectrum for the lower-level polariton mode B, while the superscript denotes the transition is from $\mathcal{N} = 1$ subspace to $\mathcal{N} = 0$ subspace. Note the transient terms and very slowly varied terms have been neglected and the base line $(\omega_A + \omega_B)/2$ for the $\mathcal{N} = 1$ subspace is added. We can observe that the eigenvalues determine the positions of the spectral component and the overlap between different states decides the intensity of the spectral lines. As a matter of fact, the spectrum is composed of three parts with equidistance but different central points δ_1, δ_2, δ_3. For each part, the interval is marked by the mechanical resonator frequency ω_m, and $(n_1 - n_2)$ with $n_1, n_2 \in [0, \infty)$ gives us a clue for numerous sidebands [61,62]. These sidebands are developed around δ_1, δ_2, δ_3, respectively, and semantically we name them as center frequencies. However, the sidebands can only be resolved when their peaks go over the height of nearby Lorentzian.

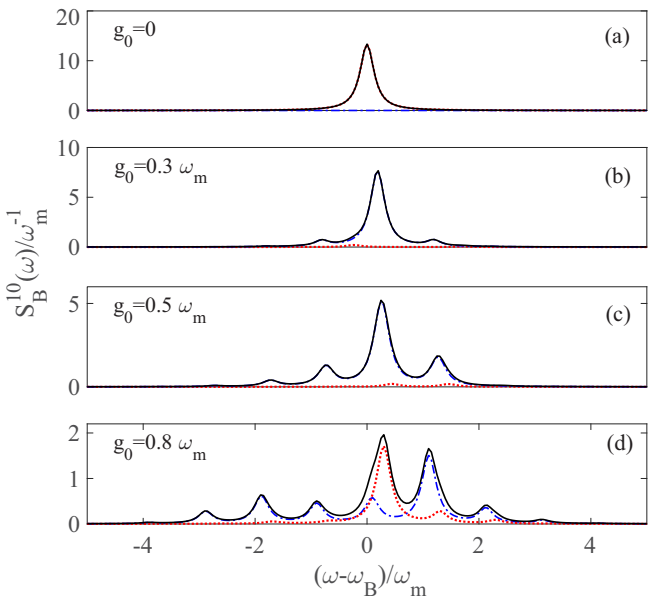

FIG. 3. Rescaled emission spectrum $S_B^{10}(\omega)/\omega_m^{-1}$ of polariton mode B (black solid curves) from $\mathcal{N}=1$ to 0 as a function of rescaled frequency detuning $(\omega-\omega_B)/\omega_m$ without the exciton-phonon coupling, i.e., $\lambda=0$, under different cavity photon-phonon coupling strength $g_0=0,\ 0.3\,\omega_m,\ 0.5\,\omega_m,\ 0.8\,\omega_m$ from (a)–(d). The black solid, blue dashed-dotted, and red dotted curves represent the rescaled $S_B^{10}(\omega)/\omega_m^{-1}$, $S_2(\omega)/\omega_m^{-1}$, and $S_3(\omega)/\omega_m^{-1}$, respectively. Other parameters are set to be: $\Delta_{ce}=0$, $\eta=0.5\,\omega_m$, $\gamma=0.15\,\omega_m$.

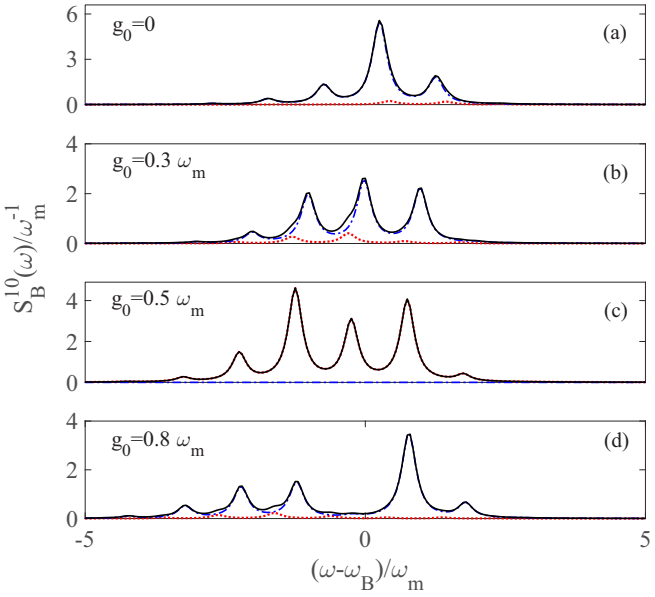

FIG. 4. Rescaled emission spectrum $S_B^{10}(\omega)/\omega_m^{-1}$ of polariton mode B (black solid curves) from $\mathcal{N}=1$ to 0 as a function of rescaled frequency detuning $(\omega-\omega_B)/\omega_m$ with the exciton-phonon coupling $\lambda=0.5\,\omega_m$, under different cavity photon-phonon coupling strength $g_0=0,\ 0.3\,\omega_m,\ 0.5\,\omega_m,\ 0.8\,\omega_m$ from (a)–(d). The black solid, blue dashed dotted, and red dotted curves represent the rescaled $S_B^{10}(\omega)/\omega_m^{-1}$, $S_2(\omega)/\omega_m^{-1}$, and $S_3(\omega)/\omega_m^{-1}$, respectively. Other parameters are set to be $\Delta_{ce}=0$, $\eta=0.5\,\omega_m$, $\gamma=0.15\,\omega_m$.

In Fig. 3, the rescaled emission spectrum $S_B^{10}(\omega)/\omega_m^{-1}$ (black solid curves) is plotted as a function of the rescaled frequency detuning $(\omega-\omega_B)/\omega_m$ with various optomechanical coupling strengths $g_0=0,\ 0.3\,\omega_m,\ 0.5\,\omega_m,\ 0.8\,\omega_m$. In order to see the effect of the mechanical resonator clearly, we first exclude the influence of exciton-phonon coupling by setting $\lambda=0$. Rescaled spectra $S_2(\omega)/\omega_m^{-1}$ and $S_3(\omega)/\omega_m^{-1}$ with central frequencies δ_2, δ_3 are plotted in the blue dashed dotted and the red dotted curves, respectively. The $S_1(\omega)$ does not show up here because we choose $n_0=2$. In this case, the initial state $|\psi(0)\rangle=|\frac{1}{2},-\frac{1}{2}\rangle|2\rangle_{\frac{1}{2},-\frac{1}{2}}$ is orthogonal to the ground state $|\psi_G^{\mathrm{GRWA}}\rangle$, i.e, $\langle\psi(0)|\psi_G^{\mathrm{GRWA}}\rangle=0$, which leads to $S_1(\omega)=0$. First, in Fig. 3(a), we consider the situation $g_0=0$ and $\lambda=0$, i.e., the polariton mode is totally decoupled with the mechanical resonator. In this case, the emission spectrum is not affected by the mechanical resonator. That is, only one Lorentzian peak appears around $\omega=\omega_B$ denoting the bare polariton mode spectrum. And it mainly comes from the contribution of $S_3(\omega)/\omega_m^{-1}$. Moreover, with the increase of optomechanical coupling strength g_0 from $0.3\,\omega_m$ to $0.8\,\omega_m$, as shown in Fig. 3(b) to Fig. 3(d), we find that the contributions of $S_2(\omega)/\omega_m^{-1}$ and $S_3(\omega)/\omega_m^{-1}$ to the rescaled total spectrum $S_B^{10}(\omega)/\omega_m^{-1}$ vary a lot. Besides, more sidebands appear at the frequency $\delta_2-n_2\omega_m$ and $\delta_3-n_2\omega_m$ for $g_0>\gamma_c$, e.g., two to six sidebands from Fig. 3(b) to Fig. 3(d), while at the expense of lower central peak. Usually, the maximum number of sidebands corresponds to the phonon number truncated for calculation (here we set as 6).

In Fig. 4, we take the exciton-phonon coupling into account, for example, $\lambda=0.5\,\omega_m$. We find that, for each specific g_0, more sidebands appear, compared to the case of $\lambda=0$ as shown in Fig. 3. Even when $g_0=0$, there are three sidebands as shown in Fig. 4(a) and it mainly comes from the contribution of $S_2(\omega)/\omega_m^{-1}$. From Figs. 3 and 4, we can find that the mechanical resonator enriches the spectrum of polariton mode with more sidebands. Moreover, when there is only parametric coupling between the polariton modes and the phonon mode, i.e., $G=g_0-\lambda=0$, the peaks of the two subseries $S_2(\omega)/\omega_m^{-1}$ and $S_3(\omega)/\omega_m^{-1}$ overlap because of the central frequency detuning $\delta_2-\delta_3=\omega_m$ in this case, as shown in Fig. 2. However, the introduction of the three-wave mixing interaction $(G=g_0-\lambda\neq 0)$ staggers the peaks of the two subseries, and leads to the staggering structure of the rescaled total emission spectrum $S_B^{10}(\omega)/\omega_m^{-1}$.

IV. BUNCHING AND ANTIBUNCHING RESONANCES OF THE POLARITON MODES

In this section, we will show how the mechanical resonator affects the statistical properties of the polariton emission. We assume that the cavity field of the hybrid system is driven by a weak classical field with the frequency ω_d. In this case, the Hamiltonian in Eq. (1) is changed into

$$H'=H+i\varepsilon(a^\dagger e^{-i\omega_d t}-ae^{i\omega_d t}). \tag{36}$$

Here, H is given in Eq. (1), and ε is the coupling strength between the cavity field and the driving field. In the rotating reference frame of the driving field under the frequency ω_d

with unitary operator $R(t) = \exp[-i\omega_d(A^\dagger A + B^\dagger B)t]$, we can write the total Hamiltonian of the system as

$$\begin{aligned}\widetilde{H}' &= \Delta_A A^\dagger A + \Delta_B B^\dagger B + \omega_m b^\dagger b \\ &\quad + (Q_A A^\dagger A + Q_B B^\dagger B)(b^\dagger + b) \\ &\quad + Q(A^\dagger B + B^\dagger A)(b^\dagger + b) \\ &\quad + i\varepsilon[\cos\theta(A^\dagger - A) - \sin\theta(B^\dagger - B)], \end{aligned} \tag{37}$$

where $\Delta_A = \omega_A - \omega_d$ ($\Delta_B = \omega_B - \omega_d$) is the detuning between the polariton mode A (B) and the driving field. For the open system, the dissipative terms in the polariton representation must be considered and can be expressed in the Lindblad superoperator form

$$\begin{aligned}\mathcal{L}_{\rm diss} &\simeq \frac{\gamma_m}{2}[(N_{\rm th}+1)\mathcal{D}[b] + N_{\rm th}\mathcal{D}[b^\dagger]] \\ &\quad + \kappa_A\mathcal{D}[A] + \kappa_B\mathcal{D}[B]. \end{aligned} \tag{38}$$

Here, the superoperator has the form of $\mathcal{D}[o]\rho = o\rho o^\dagger - \frac{1}{2}(o^\dagger o\rho + \rho o^\dagger o)$ (o can be any operator of the system, i.e., A, B, b). The first line in Eq. (38) describes the coupling of the mechanical resonator to a thermal bath, and $N_{\rm th} = 1/[\exp(\hbar\omega_m/k_BT) - 1]$ denotes the thermal phonon number at temperature T, with k_B the Boltzmann constant. $\mathcal{D}[A]$, $\mathcal{D}[B]$ represent the leakage of the polariton modes A and B with the polariton decay rates

$$\kappa_A = \kappa_a\cos^2\theta + \kappa_{ex}\sin^2\theta, \tag{39}$$

$$\kappa_B = \kappa_a\sin^2\theta + \kappa_{ex}\cos^2\theta. \tag{40}$$

Here, κ_a, κ_{ex}, and γ_m represent the decay rates of the cavity, exciton, and mechanical modes, respectively. Besides, note that the term $(\kappa_a - \kappa_{ex})^2$ has been neglected in the process of getting the decay rates κ_A and κ_B as shown in Eqs. (39) and (40) [63]. This is reasonable when the splittings of these two modes are far larger than their decay rates κ_a, κ_{ex}, which is consistent with our original assumption. Because of the high frequency of the polariton modes, we have neglected the thermal excitations of excitons and photons in the low-temperature limit. Then, the master equation for the reduced density matrix operator ρ of the whole system can be described by

$$\dot{\rho} = i[\rho, \widetilde{H}'] + \mathcal{L}_{\rm diss}\rho. \tag{41}$$

It can be solved numerically in the complete basis set $|n_A\rangle \otimes |n_B\rangle \otimes |n_b\rangle$, with n_A, n_B and $n_b = 0, 1, 2\ldots$ denoting the excitation numbers in polaritons A, B and mechanical resonator modes, respectively. In this work, the numerical calculations are done utilizing the quantum toolbox [64,65] by solving the master equation within a truncated Fock state space.

Next, we use polariton mode B as an example to show the effect of the mechanical resonator on the statistical properties of the polaritons. The equal-time second-order correlation function of polariton mode B can be given as [66]

$$g^{(2)}(0) = \frac{\langle B^\dagger B^\dagger B B\rangle}{\langle B^\dagger B\rangle^2}, \tag{42}$$

which describes the statistical properties of the polariton mode B. The status $g^{(2)}(0) < 1$ [$g^{(2)}(0) > 1$] characterizes the polariton blockade (tunneling) process, in which the polariton exhibits sub-Poisson (or super-Poisson) statistics [67–74].

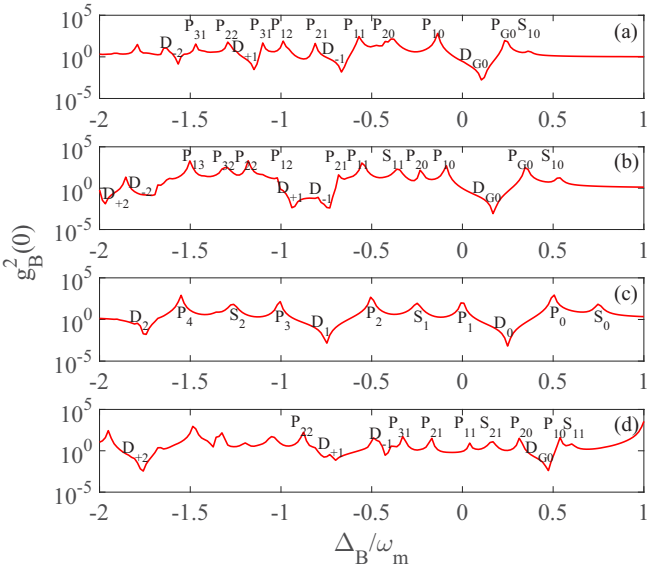

FIG. 5. The equal-time second-order correlation function $g^{(2)}(0)$ versus the rescaled detuning Δ_B/ω_m for various coupling strengths, e.g., $g_0 = 0$ in (a), $g_0 = 0.3\,\omega_m$ in (b), $g_0 = 0.5\,\omega_m$ in (c), and $g_0 = 0.8\,\omega_m$ in (d). Other parameters are $\Delta_{ce} = 0$, $\lambda = 0.5\,\omega_m$, $\eta = 0.5\,\omega_m$.

Figure 5 shows how the polariton statistics depends on dimensionless detuning Δ_B/ω_m. We note that each panel has several dips and resonant peaks, which denote the one-polariton and multipolariton resonant transition, respectively.

It will be easier to understand from the coupling balanced case $g_0 = \lambda$, which is shown in Fig. 5(c). In this case, there are only parametric couplings between the polariton modes and the phonon mode. We only need one subscript n_b ($n_b = 0, 1, 2\ldots$) to label the dips and peaks caused by different phonon number. Specifically, the dips D_{n_b} ($n_b = 0, 1, 2\ldots$) are caused by the single polariton transition from the state $|\frac{1}{2}, -\frac{1}{2}\rangle|n_b\rangle_{\frac{1}{2},-\frac{1}{2}}$ to the state $|0, 0\rangle|0\rangle$, when the detuning between the driving field and the polariton mode B satisfies the condition $\Delta_B/\omega_m = (g_0^2/\omega_m^2) - n_b$. The peaks P_{n_b} ($n_b = 0, 1, 2\ldots$) correspond to the two-polariton transition from the state $|1, -1\rangle|n_b\rangle_{1,-1}$ to the state $|0, 0\rangle|0\rangle$ when the detuning $\Delta_B/\omega_m = (2g_0^2/\omega_m^2) - (n_b/2)$. Moreover, we also label another series of peaks S_{n_b} ($n_b = 0, 1, 2\cdots$), which are the consequence of one-polarion transition from the state $|1, -1\rangle|n_b\rangle_{1,-1}$ to the state $|\frac{1}{2}, -\frac{1}{2}\rangle|0\rangle_{\frac{1}{2},-\frac{1}{2}}$ under the condition of $\Delta_B/\omega_m = (3g_0^2/\omega_m^2) - n_b$. Obviously, the distribution of these points is equally spaced, and all separated by one time or half of the frequency of the mechanical resonator ω_m in each series.

When $g_0 \neq \lambda$, the three-wave mixing interaction between A, B, and b makes the system exhibit richer nonlinearity, and the eigenstate concerning the phonon mode changes from the displaced Fock state $|n_b\rangle_{j,m}$ to their superposition as shown in Eq. (28). Thus, the positions of the dips and peaks change a lot and we introduce two subscripts to label them. As shown in Figs. 5(a), 5(b), and 5(d), we consider three different coupling

strengths $g_0 = 0, 0.3\,\omega_m$, and $0.8\,\omega_m$, respectively, and figure out the following:

(i) The dips labeled by D_{p,n_b} in Figs. 5(a), 5(b), and 5(d) are the results of one-polariton transition from the state $|\psi^{\rm GRWA}_{\frac{1}{2},p,n_b}\rangle$ to the state $|0,0\rangle|0\rangle$ at the effective detuning $\Delta'_B = \Delta_B + \eta/\sin 2\theta = -E^{\rm GRWA}_{\frac{1}{2},p,n_b}$. Note that the term $\eta/\sin 2\theta$ is added; it is because we take the base line $(\omega_A + \omega_B)/2$ for the $\mathcal{N} = 1$ subspace into account. The parameter $p = \pm$ when $n_b = 1, 2, 3\ldots$, while $p = G$ when $n_b = 0$. For example, the symbol D_{G0} labels the transition from the ground state $|\psi^{\rm GRWA}_G\rangle$ in the $\mathcal{N} = 1$ subspace to the state $|0,0\rangle|0\rangle$. The equal-time second-order correlation functions $g^{(2)}(0)$ corresponding to the dips D_{p,n_b} are smaller than 1, i.e., $g^{(2)}(0) < 1$, which means that the probability to excite the two polariton is smaller than that to excite two single polaritons independently, and then the polariton blockade happens and exhibits sub-Poisson statistics.

(ii) The peaks marked by P_{q,n_b} represent the transition from the state $|\psi^{\rm GRWA}_{1,q,n_b}\rangle$ in the subspace $\mathcal{N} = 2$ to the state $|0,0\rangle|0\rangle$ at the effective detuning $\Delta'_B = -E^{\rm GRWA}_{1,q,n_b}/2$. Here, $q = 1, 2, 3$ when $n_b = 1, 2, 3\ldots$ denoting the three energy levels in the n_bth block, while for the $n_b = 0$ block, $q = 1$, 2, and G, standing for the first- and second-excited state, and the ground state, respectively. Note that we have taken the base line $\omega_A + \omega_B$ for the $\mathcal{N} = 2$ subspace into account. Specifically, P_{10} represents two-polariton transition from the first-excited state $|\psi^{\rm GRWA}_{1,1,0}\rangle$ to $|0,0\rangle|0\rangle$ at the effective detuning $-E^{\rm GRWA}_{1,1,0}/2$, while P_{G0} represents two-polariton transition from the ground state $|\tilde{\psi}^{\rm GRWA}_G\rangle$ [Eq. (C24)] in the $\mathcal{N} = 2$ subspace to $|0,0\rangle|0\rangle$ at the effective detuning $-\tilde{E}^{\rm GRWA}_G/2$ [Eq. (C21)]. Correspondingly, the equal-time second-order correlation functions $g^{(2)}(0)$ at these peaks P_{q,n_b} are larger than 1, i.e., $g^{(2)}(0) > 1$, which means that the probability to excite the two polariton is larger than that to excite two single polaritons independently, and then the polariton tunneling happens and exhibits super-Poisson statistics.

(iii) Besides, the small peaks pointed out by S_{q,n_b} show the polariton transition between the state $|\psi^{\rm GRWA}_{1,q,n_b}\rangle$ in the $\mathcal{N} = 2$ subspace and the ground state $|\frac{1}{2},-\frac{1}{2}\rangle|0\rangle_{\frac{1}{2},-\frac{1}{2}}$ in $\mathcal{N} = 1$ subspace. In this case, the transition frequency satisfies the condition $\Delta'_B = -E^{\rm GRWA}_{1,q,n_b} + E^{\rm GRWA}_{\frac{1}{2},-\frac{1}{2},0}$. For example, S_{11} (S_{10}) denotes the transition from the state $|\psi^{\rm GRWA}_{1,1,1}\rangle$ ($|\psi^{\rm GRWA}_{1,1,0}\rangle$) in the $\mathcal{N} = 2$ subspace to the state $|\psi^{\rm GRWA}_{\frac{1}{2},-\frac{1}{2},0}\rangle$ in the $\mathcal{N} = 1$ subspace at the effective detuning $\Delta'_B = -E^{\rm GRWA}_{1,1,1}$ ($E^{\rm GRWA}_{1,1,0}$) $+ E^{\rm GRWA}_{\frac{1}{2},-\frac{1}{2},0}$.

As a summary, in the first column of Tables I and II, we list the symbols which are used to label the transitions for the balanced ($g_0 = \lambda$) and unbalanced ($g_0 \neq \lambda$) coupling cases, respectively. The transitions occur from the original states (the second column) to the final states (the third column), when the frequency detuning satisfies the conditions which are shown in the last column. We use two subscripts (q, n_b) for the unbalanced coupling case ($g_0 \neq \lambda$) when the three-mixing wave interaction is introduced, while only one (n_b) for the balanced coupling case ($g_0 = \lambda$), i.e., there are only parametric couplings between the polariton modes and the phonon mode, to discriminate different processes.

TABLE I. Symbols representing the transitions from the states shown in the second column to that in the third column for the balanced coupling case $g_0 = \lambda$. In the table, for convenience, we call the states in the second and third columns as original and final states, respectively. The last column shows the corresponding conditions which the frequency detuning Δ_B satisfies, respectively. The symbol D represents the series of dips, while P, S represent two series of peaks with one subscript n_b.

Symbol	Original state	Final state	Detuning Δ_B
D_{n_b}	$\lvert\frac{1}{2},-\frac{1}{2}\rangle\lvert n_b\rangle_{\frac{1}{2},-\frac{1}{2}}$	$\lvert 0,0\rangle\lvert 0\rangle$	$\frac{g_0^2}{\omega_m^2} - n_b$
P_{n_b}	$\lvert 1,-1\rangle\lvert n_b\rangle_{1,-1}$	$\lvert 0,0\rangle\lvert 0\rangle$	$\frac{2g_0^2}{\omega_m^2} - \frac{n_b}{2}$
S_{n_b}	$\lvert 1,-1\rangle\lvert n_b\rangle_{1,-1}$	$\lvert\frac{1}{2},-\frac{1}{2}\rangle\lvert 0\rangle_{\frac{1}{2},-\frac{1}{2}}$	$\frac{3g_0^2}{\omega_m^2} - n_b$

Furthermore, we show the equal-time second-order correlation $g^{(2)}(0)$ versus the rescaled radiation-pressure coupling strength g_0/ω_m in Fig. 6 at the given detuning $\Delta_B = g_0^2/\omega_m$. As analyzed above, for the balanced coupling case $g_0 = \lambda$, i.e., there are only parametric couplings between the polariton modes and the phonon mode, the single polariton transition from the state $|\frac{1}{2},-\frac{1}{2}\rangle|0\rangle_{\frac{1}{2},-\frac{1}{2}}$ in the $\mathcal{N} = 1$ subspace to the state $|0,0\rangle|0\rangle$ occurs. The polariton exhibits sub-Poisson statistics, i.e., the polariton blockade happens. However, the blockade is destroyed when the coupling strength satisfies the condition $g_0/\omega_m = \sqrt{n_b/2}$, which corresponds to the two-polariton transition from the state $|1,-1\rangle|n_b\rangle_{1,-1}$ in the $\mathcal{N} = 2$ subspace to the state $|0,0\rangle|0\rangle$, and can be seen in the peaks P_{n_b} as shown in Fig. 6(a). For a specific exciton-phonon coupling strength, e.g., $\lambda = 0.5\,\omega_m$ in Fig. 6(b), polariton blockade occurs once $g_0 = \lambda$, which can be seen in the dip labeled by D_0. With the increase of g_0, another two types of resonant transition occur, as labeled by P_{p,n_b} and S_{q,n_b}. Besides, for the case of $\lambda = 0.5\,g_0$, as depicted in Fig. 6(c), we observe resonant peaks labeled by S_{11}, S_{21}, P_{11}, and P_{21}. The original and final states, as well as the frequency conditions of the transition processes corresponding to these symbols, can also be found in Tables I and II, respectively. Moreover, we find that the equal-time second-order correlation function $g^{(2)}(0)$ keeps smaller than 1 in Fig. 6(a), while it remains larger than 1 in Fig. 6(c). This phenomenon may imply that the polariton blockade holding by the parametric coupling, may

TABLE II. Symbols representing the transitions from the states shown in the second column to that in the third column for the unbalanced coupling case $g_0 \neq \lambda$. In the table, for convenience, we call the states in the second and third columns as original and final states, respectively. The last column shows the corresponding conditions which the effective frequency detuning $\Delta'_B = \Delta_B + \eta/\sin 2\theta$ satisfies, respectively. The symbol D represents the series of dips, while P, S represent two series of peaks, with two subscripts p (q), n_b.

Symbol	Original state	Final state	Effective Detuning Δ'_B
D_{p,n_b}	$\lvert\psi^{\rm GRWA}_{\frac{1}{2},p,n_b}\rangle$	$\lvert 0,0\rangle\lvert 0\rangle$	$-E^{\rm GRWA}_{\frac{1}{2},p,n_b}$
P_{q,n_b}	$\lvert\psi^{\rm GRWA}_{1,q,n_b}\rangle$	$\lvert 0,0\rangle\lvert 0\rangle$	$-E^{\rm GRWA}_{1,q,n_b}/2$
S_{q,n_b}	$\lvert\psi^{\rm GRWA}_{1,q,n_b}\rangle$	$\lvert\frac{1}{2},-\frac{1}{2}\rangle\lvert 0\rangle_{\frac{1}{2},-\frac{1}{2}}$	$-E^{\rm GRWA}_{1,q,n_b} + E^{\rm GRWA}_{\frac{1}{2},-\frac{1}{2},0}$

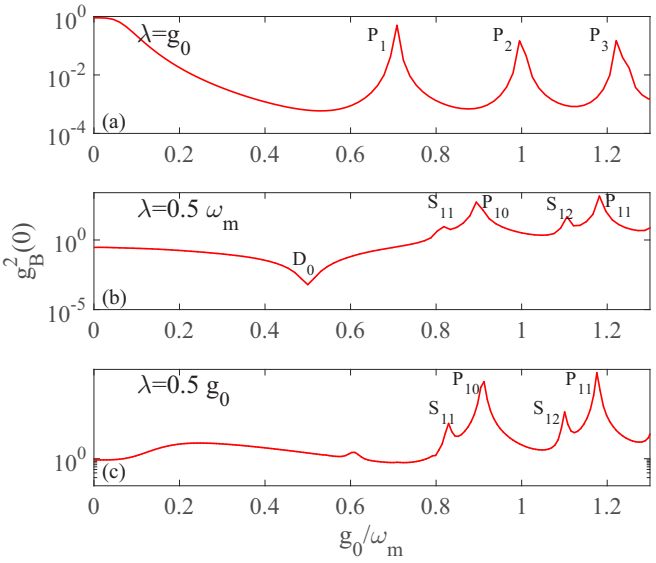

FIG. 6. The equal-time second-order correlation function $g^{(2)}(0)$ versus the rescaled coupling strength g_0/ω_m with the pump detuning $\Delta_B = g_0^2/\omega_m$ for (a) coupling balanced $\lambda = g_0$ and detuning case: (b) $\lambda = 0.5\,\omega_m$, (c) $\lambda = 0.5\,g_0$. Other parameters are $\Delta_{ce} = 0$, $\eta = 0.5\,\omega_m$.

be destroyed by the negative three-wave mixing interaction between the polariton modes and the phonon mode, at the given detuning $\Delta_B = g_0^2/\omega_m$.

V. CONCLUSIONS

In summary, we have studied a hybrid semiconductor-optomechanical system that combines the semiconducting microcavity quantum electrodynamics with optomechanics. We consider two configurations of such hybrid system in terms of the interaction between the excitons and mechanical resonator. The first one is that the vibration mirror in the cavity of the optomechanical system is considered as the semiconducting system. In this case, we assume that there is no direction coupling between the mechanical resonator and the excitons in the semiconductor mirror. The second one is that a membrane placed inside the cavity of the optomechanical system is considered as the semiconducting system. In this case, we assume that there is radiation pressure type interaction between the mechanical resonator and the excitons in the semiconductor membrane, which is realized via deformation or piezoelectric effect. In this paper, we mainly focus on the second case that the mechanical resonator, the cavity field, and the exciton are mutually interacting, i.e., the fully coupled tripartite case. The physics of the system can be described in terms of the interaction between the mechanical resonator and the polaritons, formed by the cavity photons and excitons. We also note that the research results of the second case can be easily applied to the first one by assuming that the coupling constant between the excitons and mechanical resonator is zero.

We derive analytical solutions of the eigenvalues and eigenstates of the corresponding Hamiltonian with generalized rotating-wave approximation when the total excitation numbers of the polaritons are zero, one, and two. Based on the eigenvalues and eigenstates, we further study the emission spectra and statistical properties of the polaritons, and find the rich nonlinearity occurs due to the interaction between the polaritions and mechanical resonator. For example, when the mechanical resonator is decoupled from the exciton and the cavity field, the emission spectra from one polariton to zero polarition only show a single peak. However when the mechanical resonator is coupled to both the exciton and cavity field or either one of the exciton and cavity field, the emission spectra exhibit richer structure. Under the modulation of the mechanical resonator, the emission spectrum peaks and blockade (tunneling) dips (peaks) of the polariton show many phonon sidebands, which depend on the coupling strengths of the mechanical resonator to the cavity field and the exciton. Moreover, we show how the competition between the two forms of couplings for the polariton modes and the phonon mode, i.e., parametric and three-wave mixing interactions, results in the fine emission spectra and blockade of the polaritons. We also find that the three-wave mixing interaction leads to the staggering structure of the total emission spectrum, and destroys the polariton blockade, which occurs in the parametric coupling case.

Our research results lay a theoretical foundation for the experimental study of optical, mechanical, and electrical systems, which could lead to highly sensitive and functionalized optoelectromechanical systems as discussed in Ref. [75]. Our research results may also be helpful for experimental research on the high-sensitivity displacement detection using semiconducting resonator [21], or the observation of a semiconducting band gap through mechanical displacement [26]. In particular, we show the dependence of the polariton emission spectra on the mechanical resonator. This can motivate more experiments along the research direction for controlling photons of the cavity field, phonons in vibrating mechanical resonator, and electron (or electron-hole) in an integrated platform. This hybrid system may also be applied to the quantum network for quantum information processing, e.g., the realization of quantum entanglement between different quantum objects, which is underexplored.

ACKNOWLEDGMENTS

Y.X.L. acknowledges the financial support of the National Basic Research Program of China 973 Program under Grant No. 2014CB921401, the Tsinghua University Initiative Scientific Research Program, and the Tsinghua National Laboratory for Information Science and Technology (TNList) Cross-discipline Foundation. Y. Zhang would like to acknowledge the financial support of the NSF of China under Grants No. 11474189 and No. 11674201.

APPENDIX A: SCHWINGER'S REPRESENTATIONS OF HAMILTONIAN

We find that it is convenient to obtain eigenvalues and eigenstates of the Hamiltonian in Eq. (2) using Schwinger's representation of the angular momentum for the two bosonic polariton modes A and B, which is shown in Eq. (7). For given total excitation number $\mathcal{N}$ of polaritons, the simultaneous

eigenstates of J^2 and J_z are defined as

$$|j,m\rangle = \frac{(A^\dagger)^{j+m}(B^\dagger)^{j-m}}{\sqrt{(j+m)!(j-m)!}}|0\rangle, \tag{A1}$$

with the eigenvalues $j = \mathcal{N}/2$, and $m = -\mathcal{N}/2, \ldots, \mathcal{N}/2$. In order to get more intuitive understanding, we can also express $|j,m\rangle$ as $|n_A\rangle \otimes |n_B\rangle$ in terms of polariton Fock state. That is, $|j,m\rangle = |n_A\rangle|n_B\rangle$, where

$$n_A = j + m, \quad n_B = j - m \tag{A2}$$

represent the excitation numbers in modes A and B, respectively.

APPENDIX B: EIGENVALUES AND EIGENSTATES IN $\mathcal{N} = 1$ SUBSPACE

For the $\mathcal{N} = 1$ subspace, we first consider the zeroth-order approximation which neglects the terms involving energy exchange between the phonon and the polaritons. Then, the Hamiltonian in Eq. (17) can be approximated as

$$H_3^{(0)} = \frac{1}{2}(\omega_A - \omega_B)\cos\phi\sigma_z + \omega_m N_b - \frac{1}{\omega_m}\left(\Omega + \frac{G}{2}\sigma_z\right)^2 + \frac{1}{2}(\omega_A - \omega_B)\sin\phi\sigma_x G_0(N_b). \tag{B1}$$

For the sake of clarity, we have neglected the energy baseline $(\omega_A + \omega_B)/2$. And there are only terms concerning the phonon number operator $N_b = b^\dagger b$. Thus, the Hilbert space can be decomposed into n_b manifolds in the basis of the angular momentum and mechanical resonator $|\frac{1}{2}, -\frac{1}{2}, n_b\rangle$ and $|\frac{1}{2}, \frac{1}{2}, n_b\rangle$. Based on the fact that

$$\sigma_x\left|\frac{1}{2},\frac{1}{2}\right\rangle = \left|\frac{1}{2},-\frac{1}{2}\right\rangle, \quad \sigma_x\left|\frac{1}{2},-\frac{1}{2}\right\rangle = \left|\frac{1}{2},\frac{1}{2}\right\rangle,$$
$$\sigma_y\left|\frac{1}{2},\frac{1}{2}\right\rangle = i\left|\frac{1}{2},-\frac{1}{2}\right\rangle, \quad \sigma_y\left|\frac{1}{2},-\frac{1}{2}\right\rangle = -i\left|\frac{1}{2},\frac{1}{2}\right\rangle,$$

the Hamiltonian in Eq. (B1) in the n_bth manifold takes on the form

$$H_{3,n_b}^{(0)} = \begin{bmatrix} e_{n_b}^{(1)} & \frac{B_{n_b}}{2} \\ \frac{B_{n_b}}{2} & e_{n_b}^{(2)} \end{bmatrix}, \tag{B2}$$

with

$$e_{n_b}^{(1)} = -\frac{1}{2}(\omega_A - \omega_B)\cos\phi + n_b\omega_m - \frac{\lambda^2}{\omega_m}, \tag{B3}$$

$$e_{n_b}^{(2)} = \frac{1}{2}(\omega_A - \omega_B)\cos\phi + n_b\omega_m - \frac{g_0^2}{\omega_m}, \tag{B4}$$

$$B_{n_b} = (\omega_A - \omega_B)\sin\phi G_0(n_b). \tag{B5}$$

Here, for a given phonon number n_b, the coefficient $G_0(n_b)$ is given as [48]

$$G_0(n_b) = \langle n_b|G_0(N_b)|n_b\rangle = \left\langle n_b\left|\cosh\left[\frac{G}{\omega_m}(b^\dagger - b)\right]\right|n_b\right\rangle = \exp\left(-\frac{G^2}{2\omega_m^2}\right)L_{n_b}\left(\frac{G^2}{\omega_m^2}\right). \tag{B6}$$

Here, the simple Laguerre polynomials L_{n_b} are the special case of the generalized Laguerre polynomials

$$L_n^\alpha(x) = \sum_{l=0}^{n}(-1)^l\frac{(n+\alpha)!x^l}{(n-l)!(\alpha+l)!l!} \tag{B7}$$

with the degree $n = n_b$ and index $\alpha = 0$, i.e., $L_{n_b}^0(x) = L_{n_b}(x)$. Using Eq. (B2), the eigenvalues corresponding to the Hamiltonian in Eq. (B1) can be straightforwardly given by

$$\varepsilon_{\frac{1}{2},p,n_b} = n_b\omega_m - \frac{1}{2\omega_m}\left(g_0^2 + \lambda^2\right) \pm \frac{1}{2}\sqrt{\left(e_{n_b}^{(2)} - e_{n_b}^{(1)}\right)^2 + B_{n_b}^2}, \tag{B8}$$

where $p = +$ or $p = -$ denote the two eigenvalues in the subspace of one polariton and n_b phonon excitations. The corresponding eigenstates are

$$\left|\varepsilon_{\frac{1}{2},p,n_b}\right\rangle = \frac{1}{\lambda_{\frac{1}{2},p,n_b}}\begin{pmatrix} 1 \\ \mu_{\frac{1}{2},p,n_b} \end{pmatrix} \tag{B9}$$

with

$$\mu_{\frac{1}{2},p,n_b} = \frac{2}{B_{n_b}}\left(\varepsilon_{\frac{1}{2},p,n_b} - e_{n_b}^{(1)}\right),$$
$$\lambda_{\frac{1}{2},p,n_b} = \sqrt{1 + \mu_{\frac{1}{2},p,n_b}^2}.$$

For the resonant case $(\omega_A - \omega_B)\cos\phi = \omega_m$ discussed in the main text, the single-phonon exchange terms need to be included in the first-order approximation. Thus, the Hamiltonian in Eq. (17) can be approximately written into two parts

$$H_3^{(1)} = H_{3,0}^{(1)} + H_{3,1}^{(1)}, \tag{B10}$$

with

$$H_{3,0}^{(1)} = H_3^{(0)} - \frac{1}{2}(\omega_A - \omega_B)\sin\phi\sigma_x[G_0(N_b) - \beta] \tag{B11}$$

and

$$H_{3,1}^{(1)} = \frac{1}{2}(\omega_A - \omega_B)\sin\phi\sigma_x[G_0(N_b) - \beta] + \frac{i}{2}(\omega_A - \omega_B)\sin\phi\sigma_y[F_1(N_b)b^\dagger - bF_1(N_b)]. \tag{B12}$$

Here, the parameter $\beta = G_0(0) = \exp(-G^2/2\omega_m^2)$ is introduced for the convenience of the calculations. It helps to separate the Hamiltonian $H_3^{(1)}$ in the zeroth and n_bth manifolds. The term $H_{3,0}^{(1)} - \omega_m N_b$, which can be derived from Eq. (B11), corresponds exactly to the zeroth subspace of the Hamiltonian in the zeroth-order approximation shown in Eq. (B1). Meanwhile, the Hamiltonian in n_bth manifolds is included in Eq. (B12). In the Hamiltonian $H_{3,0}^{(1)}$, the angular momentum and mechanical resonator operators are completely decoupled. And its angular momentum part can be diagonalized in the basis of $|\frac{1}{2}, -\frac{1}{2}\rangle$ and $|\frac{1}{2}, \frac{1}{2}\rangle$, by applying a unitary transformation

$$U_3 = \begin{bmatrix} \frac{1}{\lambda_-} & \frac{\mu_-}{\lambda_-} \\ \frac{1}{\lambda_+} & \frac{\mu_+}{\lambda_+} \end{bmatrix}, \tag{B13}$$

where $\lambda_\pm = \lambda_{\frac{1}{2},\pm,0}$, $\mu_\pm = \mu_{\frac{1}{2},\pm,0}$, and $\varepsilon_\pm = \varepsilon_{\frac{1}{2},\pm,0}$. Therefore, $H_{3,0}^{(1)}$ can be diagonalized into

$$\tilde{H}_{3,0}^{(1)} = U_3 H_{3,0}^{(1)} U_3^\dagger = \omega_m N_b + \begin{bmatrix} \varepsilon_- & 0 \\ 0 & \varepsilon_+ \end{bmatrix}. \tag{B14}$$

In this way, the second part $H_{3,1}^{(1)}$ of the Hamiltonian $H_3^{(1)}$ is transformed into

$$\begin{aligned} \tilde{H}_{3,1}^{(1)} &= U_3 H_{3,1}^{(1)} U_3^\dagger \\ &= \frac{1}{2} L(\omega_A - \omega_B)\sin\phi[G_0(N_b) - \beta] \\ &\quad + \frac{1}{2} M(\omega_A - \omega_B)\sin\phi[F_1(N_b)b^\dagger - bF_1(N_b)], \end{aligned} \tag{B15}$$

with

$$L = \begin{bmatrix} \frac{2\mu_-}{\lambda_-^2} & \frac{\mu_- + \mu_+}{\lambda_- \lambda_+} \\ \frac{\mu_+ + \mu_-}{\lambda_- \lambda_+} & \frac{2\mu_+}{\lambda_+^2} \end{bmatrix}, \; M = \begin{bmatrix} 0 & \frac{\mu_- - \mu_+}{\lambda_- \lambda_+} \\ \frac{\mu_+ - \mu_-}{\lambda_- \lambda_+} & 0 \end{bmatrix}.$$

The matrix elements $L_{12} = L_{21} = (\mu_- + \mu_+)/\lambda_-\lambda_+$ induce the Stark shift of the energies, which can be fully taken into account at the expense of lacking analytical expressions for the eigenvalues and will be neglected in our analytical derivation [76]. Moreover, we also neglect the counter-rotating-wave terms $\sigma_+ b^\dagger + \sigma_- b$. Thus, under the generalized rotating-wave approximation (GRWA), we can get the total Hamiltonian H_3^{GRWA}, as shown in Eq. (21). In the basis of $|\frac{1}{2}, -\frac{1}{2}, n_b\rangle$ and $|\frac{1}{2}, \frac{1}{2}, n_b - 1\rangle$ $(n_b = 1, 2, \dots)$, H_3^{GRWA} takes the following matrix form:

$$H_{3,n_b}^{\mathrm{GRWA}} = \begin{bmatrix} n_b\omega_m + \xi_{-,n_b} & \mathcal{P} \\ \mathcal{P} & (n_b - 1)\omega_m + \xi_{+,n_b-1} \end{bmatrix},$$

with

$$\begin{aligned} \xi_{\pm,n_b} &= \varepsilon_\pm + \frac{\mu_\pm}{\lambda_\pm^2}(\omega_A - \omega_B)\sin\phi[G_0(n_b) - \beta], \\ \mathcal{P} &= \frac{1}{2} M_{12}(\omega_A - \omega_B)\sin\phi R_{n_b-1,n_b}, \\ R_{n_b-1,n_b} &= \langle n_b | F_1(N_b) b^\dagger | n_b - 1\rangle \\ &= \frac{1}{\sqrt{n_b}} \frac{G}{\omega_m} \exp\left(-\frac{G^2}{2\omega_m^2}\right) L_{n_b-1}^1\left(\frac{G^2}{\omega_m^2}\right). \end{aligned}$$

APPENDIX C: EIGENVALUES AND EIGENSTATES IN $\mathcal{N} = 2$ SUBSPACE

In this appendix, we provide explicit expressions for the eigenvalues in the $\mathcal{N} = 2$ subspace. Similarly, in the zeroth-order approximation, the Hamiltonian has the form

$$\begin{aligned} H_3^{(0)} &= (\omega_A - \omega_B)\cos\phi J_z + \omega_m N_b - \frac{1}{\omega_m}(2\Omega + GJ_z)^2 \\ &\quad + (\omega_A - \omega_B)\sin\phi J_x G_0(N_b). \end{aligned} \tag{C1}$$

For the sake of clarity, we have neglected the constant term $\omega_A + \omega_B$. And the Hilbert space can be decomposed into different n_b manifolds spanned by the angular-momentum operator and oscillator basis of $|1, -1, n_b\rangle$, $|1, 0, n_b\rangle$, and $|1, 1, n_b\rangle$. For n_bth manifold, the Hamiltonian takes the form

$$H_{n_b}^{(0)} = \begin{bmatrix} e_{n_b}^{(1)} & \frac{\sqrt{2}}{2} B_{n_b} & 0 \\ \frac{\sqrt{2}}{2} B_{n_b} & e_{n_b}^{(2)} & \frac{\sqrt{2}}{2} B_{n_b} \\ 0 & \frac{\sqrt{2}}{2} B_{n_b} & e_{n_b}^{(3)} \end{bmatrix},$$

with

$$e_{n_b}^{(1)} = (\omega_B - \omega_A)\cos\phi + n_b\omega_m - \frac{1}{\omega_m}(2\Omega - G)^2, \tag{C2}$$

$$e_{n_b}^{(2)} = n_b\omega_m - \frac{1}{\omega_m}(2\Omega)^2, \tag{C3}$$

$$e_{n_b}^{(3)} = (\omega_A - \omega_B)\cos\phi + n_b\omega_m - \frac{1}{\omega_m}(2\Omega + G)^2, \tag{C4}$$

$$B_{n_b} = (\omega_A - \omega_B)\sin\phi G_0(n_b). \tag{C5}$$

The determinant of a matrix in this form gives the cubic equation $\lambda^3 + r\lambda + s = 0$ and the eigenvalue $\varepsilon = \lambda + \frac{1}{3}(e_{n_b}^{(1)} + e_{n_b}^{(2)} + e_{n_b}^{(3)})$. Here,

$$r = \frac{3ca - b^2}{3a^2}, \tag{C6}$$

$$s = \frac{2b^3 - 9abc + 27a^2 d}{27a^3} \tag{C7}$$

with

$$\begin{aligned} a &= 1, \quad b = -\left(e_{n_b}^{(1)} + e_{n_b}^{(2)} + e_{n_b}^{(3)}\right), \\ c &= e_{n_b}^{(1)} e_{n_b}^{(2)} + e_{n_b}^{(2)} e_{n_b}^{(3)} + e_{n_b}^{(3)} e_{n_b}^{(1)} - B_{n_b}^2, \\ d &= -e_{n_b}^{(1)} e_{n_b}^{(3)} e_{n_b}^{(3)} + \frac{1}{2}\left(e_{n_b}^{(3)} - e_{n_b}^{(1)}\right) B_{n_b}^2. \end{aligned}$$

Then, the corresponding eigenvalues ε_{1,q,n_b} $(q = 1, 2, 3)$ are straightforwardly given by

$$\varepsilon_{1,1,n_b} = n_b\omega_m - \frac{1}{\omega_m}\left[(2\Omega)^2 + \frac{2}{3}G^2\right] + w\chi_{1,n_b} + w^2\chi_{2,n_b},$$

$$\varepsilon_{1,2,n_b} = n_b\omega_m - \frac{1}{\omega_m}\left[(2\Omega)^2 + \frac{2}{3}G^2\right] + w^2\chi_{1,n_b} + w\chi_{2,n_b},$$

$$\varepsilon_{1,3,n_b} = n_b\omega_m - \frac{1}{\omega_m}\left[(2\Omega)^2 + \frac{2}{3}G^2\right] + \chi_{1,n_b} + \chi_{2,n_b},$$

with

$$w = \frac{1}{2}(-1 + \sqrt{3}i),$$

$$\chi_{1,n_b} = \sqrt[3]{-\frac{s}{2} + \sqrt{\left(\frac{s}{2}\right)^2 + \left(\frac{r}{3}\right)^3}},$$

$$\chi_{2,n_b} = \sqrt[3]{-\frac{s}{2} - \sqrt{\left(\frac{s}{2}\right)^2 + \left(\frac{r}{3}\right)^3}}.$$

The corresponding eigenstates

$$|\varepsilon_{1,q,n_b}\rangle = \frac{1}{\lambda_{1,q,n_b}} \begin{pmatrix} k_{1,q,n_b} \\ 1 \\ f_{1,q,n_b} \end{pmatrix},$$

where

$$k_{1,q,n_b} = \frac{\frac{\sqrt{2}}{2}B_{n_b}}{\varepsilon_{1,q,n_b} - e^{(2)}_{n_b}},$$
$$f_{1,q,n_b} = \frac{\frac{\sqrt{2}}{2}B_{n_b}}{\varepsilon_{1,q,n_b} - e^{(3)}_{n_b}},$$
$$\lambda_{1,q,n_b} = \sqrt{1 + k^2_{1,q,n_b} + f^2_{1,q,n_b}}.$$

As the first-order correction, we include the term $iJ_y[F_1(N_b)b^\dagger - bF_1(N_b)]$. The Hamiltonian now consists of two parts:

$$H^{(1)}_3 = H^{(1)}_{3,0} + H^{(1)}_{3,1}, \tag{C8}$$

with

$$H^{(1)}_{3,0} = H^{(0)}_3 - (\omega_A - \omega_B)\sin\phi J_x[G_0(N_b) - \beta] \tag{C9}$$

and

$$H^{(1)}_{3,1} = (\omega_A - \omega_B)\sin\phi J_x[G_0(N_b) - \beta] + i(\omega_A - \omega_B)\sin\phi J_y[F_1(N_b)b^\dagger - bF_1(N_b)]. \tag{C10}$$

The angular-momentum part in $H^{(1)}_{3,0}$ can be diagonalized in the basis of angular momentum in the $\mathcal{N} = 2$ subspace, i.e., $|1,-1\rangle$, $|1,0\rangle$, and $|1,1\rangle$, by a unitary matrix

$$U_4 = \begin{bmatrix} \frac{k_1}{\lambda_1} & \frac{1}{\lambda_1} & \frac{f_1}{\lambda_1} \\ \frac{k_2}{\lambda_2} & \frac{1}{\lambda_2} & \frac{f_2}{\lambda_2} \\ \frac{k_3}{\lambda_3} & \frac{1}{\lambda_3} & \frac{f_3}{\lambda_3} \end{bmatrix}. \tag{C11}$$

Then, the total Hamiltonian in the first-order approximation can be transformed into

$$\tilde{H}^{(1)}_{3,1} = U_4 H^{(1)}_{3,1} U^\dagger_4 = L(\omega_A - \omega_B)\sin\phi[G_0(N_b) - \beta] + M(\omega_A - \omega_B)\sin\phi[F_1(N_b)b^\dagger - bF_1(N_b)]. \tag{C12}$$

Here, L is a symmetric matrix with

$$L_{ii} = \frac{\sqrt{2}(k_i + f_i)}{\lambda_i^2}, \tag{C13}$$
$$L_{ij} = \frac{\sqrt{2}}{2}\frac{(k_j + f_i) + (k_i + f_j)}{\lambda_i\lambda_j}, \tag{C14}$$

while M is an antisymmetric one with

$$M_{ij(i<j)} = \frac{\sqrt{2}}{2}\frac{(k_i + f_j) - (k_j + f_i)}{\lambda_i\lambda_j}. \tag{C15}$$

Once again, we neglect the static shift of the mechanical resonator which can be fully taken into account at the expense of losing analytical expressions for the eigenvalues and eigenvectors using Braak's method [76]. Besides, by neglecting the remote matrix elements $L_{1,3}$, $L_{3,1}$, $M_{1,3}$, $M_{3,1}$ and the counter-rotating-wave terms, i.e., $J_+b^\dagger + J_-b$, we can arrive at the total Hamiltonian

$$\begin{aligned} H^{\mathrm{GRWA}}_3 = {} & \omega_m b^\dagger b + \xi_{1,N_b}|1,-1\rangle\langle 1,-1| + \xi_{2,N_b}|1,0\rangle\langle 1,0| \\ & + \xi_{3,N_b}|1,1\rangle\langle 1,1| \\ & + M_{12}(\omega_A - \omega_B)\sin\phi F_1(N_b)(b^\dagger|1,-1\rangle\langle 1,0| \\ & + b|1,0\rangle\langle 1,-1|) \\ & + M_{23}(\omega_A - \omega_B)\sin\phi F_1(N_b)(b^\dagger|1,0\rangle\langle 1,1| \\ & + b|1,1\rangle\langle 1,0|) \end{aligned} \tag{C16}$$

with

$$\xi_{i,N_b} = \varepsilon_i + (\omega_A - \omega_B)L_{ii}\sin\phi[G_0(N_b) - \beta]. \tag{C17}$$

The individual bosonic creation (annihilation) operator $b^\dagger$ (b) also appears in the GRWA, so the transitions between states belonging to different manifolds should be involved. In the basis of $|1,-1,n_b+1\rangle$, $|1,0,n_b\rangle$, and $|1,1,n_b-1\rangle$ ($n_b = 1,2,\dots$), the Hamiltonian in the n_bth block $H^{\mathrm{GRWA}}_{3,n_b}$ takes the following matrix form:

$$H^{\mathrm{GRWA}}_{3,n_b} = n_b\omega_m + \begin{bmatrix} \xi_{1,n_b+1} + \omega_m & \mathcal{P} & 0 \\ \mathcal{P} & \xi_{2,n_b} & \mathcal{D} \\ 0 & \mathcal{D} & \xi_{3,n_b-1} - \omega_m \end{bmatrix},$$

where

$$\mathcal{P} = M_{12}(\omega_A - \omega_B)\sin\phi R_{n_b,n_b+1},$$
$$\mathcal{D} = M_{23}(\omega_A - \omega_B)\sin\phi R_{n_b-1,n_b},$$
$$\xi_{i,n_b} = \varepsilon_i + (\omega_A - \omega_B)L_{ii}\sin\phi[G_0(n_b) - \beta].$$

Then, the eigenvalues can be obtained as

$$\begin{aligned} E^{\mathrm{GRWA}}_{1,1,n_b} &= n_b\omega_m + \frac{1}{3}\left(\xi_{1,n_b+1} + \xi_{2,n_b} + \xi_{3,n_b-1}\right) + \mathcal{Q}_1, \\ E^{\mathrm{GRWA}}_{1,2,n_b} &= n_b\omega_m + \frac{1}{3}\left(\xi_{1,n_b+1} + \xi_{2,n_b} + \xi_{3,n_b-1}\right) + \mathcal{Q}_2, \\ E^{\mathrm{GRWA}}_{1,3,n_b} &= n_b\omega_m + \frac{1}{3}\left(\xi_{1,n_b+1} + \xi_{2,n_b} + \xi_{3,n_b-1}\right) + \mu_{1,n_b} + \mu_{2,n_b}, \end{aligned} \tag{C18}$$

with

$$\mathcal{Q}_1 = \min\left(w\mu_{1,n_b} + w^2\mu_{2,n_b}, w^2\mu_{1,n_b} + w\mu_{2,n_b}\right),$$
$$\mathcal{Q}_2 = \max\left(w\mu_{1,n_b} + w^2\mu_{2,n_b}, w^2\mu_{1,n_b} + w\mu_{2,n_b}\right).$$

Note that here we present the eigenvalues in ascending order. The parameter μ_{i,n_b} can be obtained with the same process as χ_{i,n_b} by solving the cubic equation. And the corresponding eigenstate has the form

$$\left|\varphi^{\mathrm{GRWA}}_{1,q,n_b}\right\rangle = \frac{1}{\Lambda_{1,q,n_b}}(K_{-1,q,n_b}|1,-1,n_b+1\rangle + |1,0,n_b\rangle + F_{1,q,n_b}|1,1,n_b-1\rangle), \tag{C19}$$

with

$$K_{1,q,n_b} = \frac{\mathcal{P}}{E^{\mathrm{GRWA}}_{1,q,n_b} - [(n_b+1)\omega_m + \xi_{1,n_b+1}]},$$
$$F_{1,q,n_b} = \frac{\mathcal{D}}{E^{\mathrm{GRWA}}_{1,q,n_b} - [(n_b-1)\omega_m + \xi_{3,n_b-1}]},$$
$$\Lambda_{1,q,n_b} = \sqrt{1 + K^2_{1,q,n_b} + F^2_{1,q,n_b}}.$$

There is a special case for $n_b = 0$. In the basis of $|1,-1,1\rangle$ and $|1,0,0\rangle$, the Hamiltonian in this block can be written as

$$H^{\mathrm{GRWA}}_{3,0} = \begin{bmatrix} \omega_m + \xi_{1,1} & X \\ X & \xi_{2,0} \end{bmatrix},$$

with $X = M_{12}(\omega_A - \omega_B)\sin\phi R_{0,1}$, and the eigenvalues are given by

$$E^{\mathrm{GRWA}}_{1,q,0} = \tfrac{1}{2}(\omega_m + \xi_{1,1} + \xi_{2,0}) \pm \tfrac{1}{2}\sqrt{(\omega_m + \xi_{1,1} - \xi_{2,0})^2 + 4X^2}, \tag{C20}$$

with $q = 1, 2$ denoting eigenvalues of the first and second excited states, respectively. The ground state is $|1,-1,0\rangle$ with energy

$$\tilde{E}^{\mathrm{GRWA}}_G = \xi_{-,0} = \varepsilon_- = -\frac{1}{\omega_m}\left[(2\Omega)^2 + \frac{2}{3}G^2\right] + \chi_{1,0} + \chi_{2,0}. \tag{C21}$$

The eigenstates to the original Hamiltonian have the form

$$\left|\psi^{\mathrm{GRWA}}_{1,q,n_b}\right\rangle = U_1^\dagger U_2^\dagger U_4^\dagger \left|\varphi^{\mathrm{GRWA}}_{1,q,n_b}\right\rangle = U_1^\dagger \begin{bmatrix} |1,-1\rangle \frac{1}{\Lambda_{1,q,n_b}}\left(\frac{k_1}{\lambda_1}K_{-1,q,n_b}|n_b+1\rangle_{1,-1} + \frac{k_2}{\lambda_2}|n_b\rangle_{1,-1} + \frac{k_3}{\lambda_3}F_{1,q,n_b}|n_b-1\rangle_{1,-1}\right) \\ +|1,0\rangle \frac{1}{\Lambda_{1,q,n_b}}\left(\frac{K_{-1,q,n_b}}{\lambda_1}|n_b+1\rangle_{1,0} + \frac{1}{\lambda_2}|n_b\rangle_{1,0} + \frac{F_{1,q,n_b}}{\lambda_3}|n_b-1\rangle_{1,0}\right) \\ +|1,1\rangle \frac{1}{\Lambda_{1,q,n_b}}\left(\frac{f_1}{\lambda_1}K_{-1,q,n_b}|n_b+1\rangle_{1,1} + \frac{f_2}{\lambda_2}|n_b\rangle_{1,1} + \frac{f_3}{\lambda_3}F_{1,q,n_b}|n_b-1\rangle_{1,1}\right) \end{bmatrix}. \tag{C22}$$

Here, $n_b = 1, 2, 3\ldots$ and $q = 1, 2, 3$. On the other hand, for $n_b = 0$, the first- and second-excited eigenstates are labeled by

$$\left|\psi^{\mathrm{GRWA}}_{1,q,0}\right\rangle = U_1^\dagger U_2^\dagger U_5^\dagger \left|\varphi^{\mathrm{GRWA}}_{1,q,0}\right\rangle = U_1^\dagger \frac{1}{\Lambda_{1,q,0}} \begin{bmatrix} |1,-1\rangle\left(\frac{1}{\Lambda_{1,-,0}}|1\rangle_{1,-1} + \frac{\Upsilon_{1,q,0}}{\Lambda_{1,+,0}}|0\rangle_{1,-1}\right) \\ +|1,0\rangle\left(\frac{\Upsilon_{1,1,0}}{\Lambda_{1,1,0}}|1\rangle_{1,0} + \frac{\Upsilon_{1,2,0}}{\Lambda_{1,2,0}}\Upsilon_{1,q,0}|0\rangle_{1,0}\right) \end{bmatrix}, \tag{C23}$$

with $q = 1, 2$ and

$$U_5 = \begin{bmatrix} \frac{1}{\Lambda_{1,1,0}} & \frac{\Upsilon_{1,1,0}}{\Lambda_{1,1,0}} \\ \frac{1}{\Lambda_{1,2,0}} & \frac{\Upsilon_{1,2,0}}{\Lambda_{1,2,0}} \end{bmatrix},$$

$$\Upsilon_{1,q,0} = \frac{1}{X}\left[E^{\mathrm{GRWA}}_{1,q,0} - (\omega_m + \xi_{1,1})\right], \quad \Lambda_{1,q,0} = \sqrt{1 + \Upsilon^2_{1,q,0}}.$$

The eigenstate corresponding to the ground state is

$$\left|\tilde{\psi}^{\mathrm{GRWA}}_G\right\rangle = U_1^\dagger U_2^\dagger |1,-1,0\rangle = \sin^2\frac{\phi}{2}|1,1\rangle|0\rangle_{1,-1} + \frac{\sin\phi}{\sqrt{2}}|1,0\rangle|0\rangle_{1,-1} + \cos^2\frac{\phi}{2}|1,-1\rangle|0\rangle_{1,-1}. \tag{C24}$$

[1] T. J. Kippenberg and K. J. Vahala, Science **321**, 1172 (2008).
[2] J. D. Thompson, B. M. Zwickl, A. M. Jayich, F. Marquardt, S. M. Girvin, and J. G. E. Harris, Nature (London) **452**, 72 (2008).
[3] F. Marquardt and S. M. Girvin, Physics **2**, 40 (2009).
[4] M. Aspelmeyer, P. Meystre, and K. Schwab, Phys. Today **65**(7), 29 (2012).
[5] M. Aspelmeyer, T. J. Kippenberg, and F. Marquardt, Rev. Mod. Phys. **86**, 1391 (2014).
[6] Y. L. Liu, C. Wang, J. Zhang, and Y. X. Liu, Chin. Phys. B **27**, 024204 (2018).
[7] H. Ian, Z. R. Gong, Y. X. Liu, C. P. Sun, and F. Nori, Phys. Rev. A **78**, 013824 (2008).
[8] Y. Chang, T. Shi, Y. X. Liu, C. P. Sun, and F. Nori, Phys. Rev. A **83**, 063826 (2011).
[9] H. Jing, D. S. Goldbaum, L. Buchmann, and P. Meystre, Phys. Rev. Lett. **106**, 223601 (2011).
[10] H. Wang, H. C. Sun, J. Zhang, and Y. X. Liu, Sci. China Phys., Mech. Astron. **55**, 2264 (2012).
[11] H. Jing, X. Zhao, and L. F. Buchmann, Phys. Rev. A **86**, 065801 (2012).

[12] I. Wilson-Rae, P. Zoller, and A. Imamoğlu, Phys. Rev. Lett. **92**, 075507 (2004).
[13] J. Restrepo, C. Ciuti, and I. Favero, Phys. Rev. Lett. **112**, 013601 (2014).
[14] B.-Y. Zhou and G.-X. Li, Phys. Rev. A **94**, 033809 (2016).
[15] M. Cotrufo, A. Fiore, and E. Verhagen, Phys. Rev. Lett. **118**, 133603 (2017).
[16] L. Tian, Phys. Rev. B **84**, 035417 (2011).
[17] T. Ramos, V. Sudhir, K. Stannigel, P. Zoller, and T. J. Kippenberg, Phys. Rev. Lett. **110**, 193602 (2013).
[18] H. Wang, X. Gu, Y. X. Liu, A. Miranowicz, and F. Nori, Phys. Rev. A **90**, 023817 (2014).
[19] H. Wang, X. Gu, Y. X. Liu, A. Miranowicz, and F. Nori, Phys. Rev. A **92**, 033806 (2015).
[20] J. Restrepo, I. Favero, and C. Ciuti, Phys. Rev. A **95**, 023832 (2017).
[21] L. Ding, C. Baker, P. Senellart, A. Lemaitre, S. Ducci, G. Leo, and I. Favero, Phys. Rev. Lett. **105**, 263903 (2010).
[22] J. Liu, K. Usami, A. Naesby, T. Bagci, E. S. Polzik, P. Lodahl, and S. Stobbe, Appl. Phys. Lett. **99**, 243102 (2011).
[23] T. Watanabe, H. Okamoto, K. Onomitsu, H. Gotoh, T. Sogawa, and H. Yamaguchi, Appl. Phys. Lett. **101**, 082107 (2012).
[24] A. Xuereb, K. Usami, A. Naesby, E. S. Polzik, and K. Hammerer, New J. Phys. **14**, 085024 (2012).
[25] E. Gil-Santos, M. Labousse, C. Baker, A. Goetschy, W. Hease, C. Gomez, A. Lemaitre, G. Leo, C. Ciuti, and I. Favero, Phys. Rev. Lett. **118**, 063605 (2017).
[26] K. Usami, A. Naesby, T. Bagci, B. Melholt Nielsen, J. Liu, S. Stobbe, P. Lodahl, and E. S. Polzik, Nat. Phys. **8**, 168 (2012).
[27] M. Mitchell, A. C. Hryciw, and P. E. Barclay, Appl. Phys. Lett. **104**, 141104 (2014).
[28] I. Yeo, P.-L. deAssis, A. Gloppe, E. Dupont-Ferrier, P. Verlot, N. S. Malik, E. Dupuy, J. Claudon, J. M. Gerard, A. Auffeves, G. Nogues, S. Seidelin, J.-Ph. Poizat, O. Arcizet, and M. Richard, Nat. Nanotechnol. **9**, 106 (2014).
[29] M. Montinaro, G. Wüst, M. Munsch, Y. Fontana, E. Russo-Averchi, M. Heiss, A. Fontcuberta i Morral, R. J. Warburton, and M. Poggio, Nano Lett. **14**, 4454 (2014).
[30] H. Okamoto, D. Ito, K. Onomitsu, H. Sanada, H. Gotoh, T. Sogawa, and H. Yamaguchi, Phys. Rev. Lett. **106**, 036801 (2011).
[31] H. Okamoto, D. Ito, T. Watanabe, K. Onomitsu, H. Sanada, H. Gotoh, T. Sogawa, and H. Yamaguchi, Phys. Rev. B **84**, 014305 (2011).
[32] R. Ohta, H. Okamoto, T. Tawara, H. Gotoh, and H. Yamaguchi, Phys. Rev. Lett. **120**, 267401 (2018).
[33] C. Weisbuch, M. Nishioka, A. Ishikawa, and Y. Arakawa, Phys. Rev. Lett. **69**, 3314 (1992).
[34] A. Verger, C. Ciuti, and I. Carusotto, Phys. Rev. B **73**, 193306 (2006).
[35] I. Carusotto, Michiel Wouters, and C. Ciuti, J. Low Temp. Phys. **148**, 459 (2007).
[36] Y. Todorov, A. M. Andrews, R. Colombelli, S. De Liberato, C. Ciuti, P. Klang, G. Strasser, and C. Sirtori, Phys. Rev. Lett. **105**, 196402 (2010).
[37] J. J. Hopfield, Phys. Rev. **112**, 1555 (1958).
[38] C. Q. Cao, H. Cao, and Y. X. Liu, Phys. Rev. B **62**, 16453 (2000).
[39] C.-Q. Cao, H. Cao, and Y.-X. Liu, Phys. Rev. B **63**, 199901 (2001).
[40] G. R. Jin, P. Zhang, Y. X. Liu, and C. P. Sun, Phys. Rev. B **68**, 134301 (2003).
[41] L. Sapienza, A. Vasanelli, C. Ciuti, C. Manquest, and C. Sirtori, Appl. Phys. Lett. **90**, 201101 (2007).
[42] V. Savona, C. Piermarocchi, A. Quattropani, P. Schwendimann, and F. Tassone, Phase Transitions **68**, 169 (1999).
[43] C. Ciuti, P. Schwendimann, and A. Quattropani, Semicond. Sci. Technol. **18**, S279 (2003).
[44] G. Rozas, A. E. Bruchhausen, A. Fainstein, B. Jusserand, and A. Lemaitre, Phys. Rev. B **90**, 201302(R) (2014).
[45] B. Jusserand, A. N. Poddubny, A. V. Poshakinskiy, A. Fainstein, and A. Lemaitre, Phys. Rev. Lett. **115**, 267402 (2015).
[46] O. Kyriienko, T. C. H. Liew, and I. A. Shelykh, Phys. Rev. Lett. **112**, 076402 (2014).
[47] E. A. Sete, H. Eleuch, and C. H. Raymond Ooi, Phys. Rev. A **92**, 033843 (2015).
[48] E. K. Irish, Phys. Rev. Lett **99**, 173601 (2007).
[49] L. C. Beidenharn and J. D. Louck, *Angular Momentum in Quantum Physics* (Addison-Wesley, London, 1981), pp. 205–264.
[50] F. A. M. de Oliveira, M. S. Kim, P. L. Knight, and V. Buzek, Phys. Rev. A **41**, 2645 (1990).
[51] Y. X. Liu, C. P. Sun, S. X. Yu, and D. L. Zhou, Phys. Rev. A **63**, 023802 (2001).
[52] Y. X. Liu, N. Imoto, Ş. K. Özdemir, G. R. Jin, and C. P. Sun, Phys. Rev. A **65**, 023805 (2002).
[53] S. Ashhab and F. Nori, Phys. Rev. A **81**, 042311 (2010).
[54] S. Agarwal, S. M. Hashemi Rafsanjani, and J. H. Eberly, Phys. Rev. A **85**, 043815 (2012).
[55] L. J. Mao, S. N. Huai, and Y. B. Zhang, J. Phys. A: Math. Theor. **48**, 345302 (2015).
[56] L. J. Mao, Y. X. Liu, and Y. B. Zhang, Phys. Rev. A **93**, 052305 (2016).
[57] Y. Y. Zhang and Q. H. Chen, Phys. Rev. A **91**, 013814 (2015).
[58] Y. Y. Zhang, X. Y. Chen, S. He, and Q. H. Chen, Phys. Rev. A **94**, 012317 (2016).
[59] R. J. Glauber, Phys. Rev. **131**, 2766 (1963).
[60] J. H. Eberly and K. Wodkiewice, J. Opt. Soc. Am. **67**, 1252 (1977).
[61] P. Rabl, Phys. Rev. Lett **107**, 063601 (2011).
[62] J. Q. Liao, H. K. Cheung, and C. K. Law, Phys. Rev. A **85**, 025803 (2012).
[63] X. Zhang, C.-L. Zou, L. Jiang, and H. X. Tang, Cavity magnomechanics, Sci. Adv. **2**, e1501286 (2016).
[64] J. R. Johansson, P. D. Nation, and F. Nori, Comput. Phys. Commun. **183**, 1760 (2012).
[65] J. R. Johansson, P. D. Nation, and F. Nori, Comput. Phys. Commun. **184**, 1234 (2013).
[66] M. O. Scully and M. S. Zubairy, *Quantum Optics* (Cambridge University Press, Cambridge, 1997).
[67] L. Tian and H. J. Carmichael, Phys. Rev. A **46**, R6801 (1992).
[68] A. Imamoglu, H. Schmidt, G. Woods, and M. Deutsch, Phys. Rev. Lett. **79**, 1467 (1997).
[69] K. M. Birnbaum, A. Boca, R. Miller, A. D. Boozer, T. E. Northup, and H. J. Kimble, Nature (London) **436**, 87 (2005).
[70] A. Miranowicz, M. Paprzycka, Y. X. Liu, J. Bajer, and F. Nori, Phys. Rev. A **87**, 023809 (2013).

[71] X. W. Xu, Y. J. Li, and Y. X. Liu, Phys. Rev. A **87**, 025803 (2013).
[72] X. W. Xu, H. Wang, J. Zhang, and Y. X. Liu, Phys. Rev. A **88**, 063819 (2013).
[73] Y. X. Liu, X. W. Xu, A. Miranowicz, and F. Nori, Phys. Rev. A **89**, 043818 (2014).
[74] Y. L. Liu, G. Z. Wang, Y. X. Liu, and F. Nori, Phys. Rev. A **93**, 013856 (2016).
[75] M. Asano, R. Ohta, T. Yamamoto, H. Okamoto, and H. Yamaguchi, Appl. Phys. Lett. **112**, 201103 (2018).
[76] D. Braak, Phys. Rev. Lett. **107**, 100401 (2011).